Simulating Nitric Oxide in the Lower Thermosphere using a 3D Model

Karthik Venkataramani

Thesis submitted to the Faculty of the
Virginia Polytechnic Institute and State University
in partial fulfillment of the requirements for the degree of

Master of Science
in
Electrical Engineering

Scott M. Bailey, Chair
Wayne A. Scales
Gregory D. Earle

December 2, 2011
Blacksburg, Virginia

Keywords: Nitric Oxide, TIEGCM, $N_2(A)$, Thermospheric modelling, Simulating NO.

Simulating Nitric Oxide in the Lower Thermosphere using a 3D Model

Karthik Venkataramani

ABSTRACT

Nitric oxide (NO), despite being a minor species, influences the chemistry, composition and energy balance of the earth's atmosphere above 90 kilometers. Variations in its density have been shown to strongly correlate with solar x-ray irradiance at lower latitudes and precipitating energetic particles at higher latitudes. Though the broad variations in NO densities with altitude and latitude are well known, there are still uncertainties associated with its chemistry. It is important to accurately model NO and its associated chemistry in an atmospheric model in order to obtain an accurate representation of the thermosphere.

The NCAR Thermosphere-Ionosphere-Electrodynamics General Circulation Model (TIEGCM) is a three dimensional first principles based model which includes a self consistent aeronomic scheme that solves for winds, temperatures and densities of various neutral and charged species in the earth's upper atmosphere. Using a combination of the solar irradiance spectrum and solar indices as inputs, the model computes these outputs at every time step.

The ability of the TIEGCM to predict NO densities in the thermosphere is examined by comparing results from the model with data obtained from the Student Nitric Oxide Explorer (SNOE). The comparisons are made for the year 1999 at 110 km and 150 km at the equator. Changes are made to the NO chemistry present in the model to reflect recent results obtained from laboratory data. Paricularly, the reaction of atomic oxygen with the first excited electronic state of nitrogen, $N_2(A)$ has been shown to play an important role in the production of NO. These changes are introduced to the model and their effect on NO densities is studied.

Overall, it is seen that the updated chemistry scheme reduces the model agreement with the SNOE data at 110 km while slightly improving the agreement at a 150 km. The loss of agreement at 110 km is attributed to the fact that the neutral temperatures and atomic oxygen densities calculated by the TIEGCM are in sharp disagreement to the temperatures predicted by the NRL-MSIS at a 110 km, on which the new chemistry scheme is based.

While the chemistry scheme used in this thesis is a step in the right direction for modelling NO using the TIEGCM, the parameters used were determined from the best fit obtained from the 1-D NO model. In the light of the differences between the NRL-MSIS and TIEGCM, it is necessary to return to the laboratory data and modify the parameters used here to achieve a better agreement with the data.

Dedicated to,

Sunny days and a cup of tea -

May you never find one without the other.

Contents

1 Introduction **1**

1.1 Nitric Oxide in the lower thermosphere 2

1.2 Thermospheric Modelling of NO 5

1.3 Overview of Thesis 8

2 Description of the TIEGCM **9**

2.1 Equations 10

2.2 Inputs 11

2.2.1 Solar Input 12

2.2.2 Magnetospheric Inputs 12

2.2.3 Boundary Conditions 13

2.3 Outputs 14

3 Modifying the TIEGCM **15**

3.1 Modified branching ratios 16

3.1.1 $NO^+ + e \rightarrow 0.95N(^2D) + 0.05N(^4S) + O$ 16

3.1.2 $N_2^+ + e \rightarrow 1.52N(^2D) + 0.48N(^4S)$ 16

3.1.3 $N_2 + hv/e^* \rightarrow 0.5N(^2D) + 0.5N(^4S)$ 17

3.2 Modified rate coefficients 17

3.2.1 $N(^4S) + NO \rightarrow N_2 + O$ 17

3.2.2 $N(^2D) + O_2 \rightarrow NO + O$ 19

3.2.3 $N(^2D) + O \rightarrow N(^4S) + O$ 20

3.3 Other changes 21

3.3.1 $N^+ + O_2 \rightarrow N(^2D) + O_2^+$ 21

3.3.2 $N(^2D) + N_2 \rightarrow N(^4S) + N_2$ 23

3.4 $N_2(A)$ Chemistry 23

3.5 Summary 25

4 Results **27**

4.1 SNOE 27

4.2 Overview of the chemistry 28

4.3 Model-Data Comparisons 29

4.3.1 $NO^+ + e \rightarrow 0.95N(^2D) + 0.05N(^4S) + O$ 30

4.3.2 $N_2^+ + e \rightarrow 1.52N(^2D) + 0.48N(^4S)$ 32

4.3.3 $N_2 + hv/e^* \rightarrow 0.5N(^2D) + 0.5N(^4S)$ 34

4.3.4 $N(^4S) + NO \rightarrow N_2 + O$ 36

4.3.5 $N(^2D) + O_2 \rightarrow NO + O$ 38

4.3.6 $N(^2D) + O \rightarrow N(^4S) + O$ 40

4.3.7 $N^+ + O_2 \rightarrow N(^2D) + O_2^+$ 42

4.3.8 $N(^2D) + N_2 \rightarrow N(^4S) + N_2$ 44

4.3.9 $N_2(A)$ Chemistry, $N_2(A) + O \rightarrow NO + N(^2D)$ 46

4.3.10 Overall effect of updated chemistry 49

5 Conclusions **54**

List of Figures

1.1 NO number densities by SNOE and TIEGCM at 110 km at the equator, 1999. 6

1.2 NO number densities by SNOE and TIEGCM at 150 km at the equator, 1999. 7

3.1 Reaction rates for $N(^4S) + NO \rightarrow N_2 + O$ 18

3.2 Reaction rates for $N(^2D) + O_2 \rightarrow NO + O$ 19

3.3 Reactions rates for $N(^2D) + O \rightarrow N(^4S) + O$ 21

3.4 N_2 mass mixing ratios at 110 km & 150 km v/s time, and the linear fit used for scaling the N_2^+ production rate to the N_2(A) production 25

4.1 Modified branching ratio for $ra1$, effect at 110 km 30

4.2 Modified branching ratio for $ra1$, effect at 150 km 31

4.3 Modified branching ratio for $ra3$, effect at 110 km 32

4.4 Modified branching ratio for $ra1$, effect at 150 km 33

4.5 Modified branching ratio $brn2d$, effect at 110 km 34

4.6 Modified branching ratio $brn2d$, effect at 150 km 35

4.7 Changed temperature dependence of reaction rate $beta3$, effect at 110 km . . 36

4.8 Changed temperature dependence of reaction rate $beta3$, effect at 150 km . . 37

4.9 Added temperature dependence of reaction rate *beta*2, effect at 110 km . . . 38

4.10 Added temperature dependence of reaction rate *beta*2, effect at 150 km . . . 39

4.11 Added temperature dependence of reaction rate *beta*4, effect at 110 km . . . 40

4.12 Added temperature dependence of reaction rate *beta*4, effect at 150 km . . . 41

4.13 $N^+ + O_2 \rightarrow N(^2D) + O_2^+$, increased $N(^2D)$ yield 42

4.14 $N^+ + O_2 \rightarrow N(^2D) + O_2^+$, increased $N(^2D)$ yield 43

4.15 Introduced new reaction, effect at 110 km 44

4.16 Introduced new reaction, effect at 150 km 45

4.17 $N_2(A)$ chemistry, effect at 110 km 46

4.18 Atomic oxygen densities in NRL-MSIS & TIEGCM at 110 km 47

4.19 $N_2(A)$ chemistry, effect at 150 km 48

4.20 Updated chemistry scheme at 110 km 49

4.21 Updated chemistry scheme at 150 km 50

4.22 Comparison of neutral temperatures in NRL-MSIS and TIEGCM at 110 km 51

4.23 Comparison of neutral temperatures in NRL-MSIS and TIEGCM at 110 km 52

List of Tables

3.1 Current TIEGCM Modifications 26

5.1 Future TIEGCM Modifications 55

Acknowledgements

I would like to begin by thanking my parents, for all that they mean to me. For their trust and infinite patience with me, for providing me with all the opportunities that they have, for guiding and supporting me as I tottered through my academic career. They have taught me the lessons of virtue and patience, which I hold as valuable beyond all.

This thesis and my Master's degree would not exist if it were not for my advisor, Dr. Scott Bailey. His patience and faith in me are undoubtedly the two main reasons that re-inforced my own beliefs in my choice of graduate studies, which have helped me come this far both as a student and an individual. His ability to look at the best of things during the worst of times is something that I admire greatly, and hope to emulate in my own career.

My labmates, Justin Carstens, Cissi, Padma and Brentha - I owe you all so much more than just an acknowledgement! I have been extremely lucky to have found friends in all of you - I am sure my enthusiasm to come in to the lab in the morning wouldn't have been half as much if it didn't mean working with you guys and discussing science, math, philosophy and language!

A special word of thanks to Justin Yonker is in order here. More than once he went out of his way to guide and help me, and I am grateful towards the physics, chemistry, IDL, LaTeXand guitar lessons that he unflinchingly provided in the face of looming deadlines despite his lack of sleep. He has guided me throughout my research and my thesis writing with his ideas and suggestions, and his attention to detail never ceases to amaze me. I hope some of it rubs off

on me. Also, thanks for the Phish concert!

A word of thanks to my family, both near and far (geographically, not emotionally). These past two and a half years have been interesting to say the least, and I thank you all for being there to provide a constant emotional and moral helpline with anecdotes and reminders that beyond all of this, there is a place called home.

And you patient reader, must be a dear friend (I assume everyone else has left my thesis in a non-descript corner by now). Yes, you. Sitting there, with a smile slowly creeping upon your face, in memory of that which we have been through. In memory of dinners on the floor, free pizza, raquetball matches, subway, broken glass panes, monopoly, birthdays and music. Lest it be unsaid, I will cherish these memories for a long, long time to come. I tip my hat to you, Sir - so long, until we meet again.

Chapter 1

Introduction

The main purpose of this thesis is to look at the ability of the current version of the Thermosphere-Ionosphere-Electrodynamics General Circulation Model (TIEGCM) [1] to model Nitric Oxide (NO) in the lower thermosphere. Efforts are directed towards examining the chemistry contained in the model, and improving the model's ability to predict the NO density in the thermosphere. This thesis also tries to serve as a handbook of sorts for the use of the TIEGCM model, and briefly outlines the steps involved in both setting up the model and changing the code contained in it to reflect the updated chemistry scheme used in this thesis. The data from the Student Nitric Oxide Explorer (SNOE) [2] is the reference against which the results from the model are compared.

This chapter is intended towards introducing the reader to thermosphere, nitric oxide and terminology associated with it. The importance of nitric oxide in the atmosphere, despite it being a minor species is discussed below, and this is emphasized by presenting the relevant chemistry. The topic of atmospheric modelling is introduced in light of the TIEGCM followed by a brief description of it; Preliminary comparisons between SNOE data and the TIEGCM results are presented to give the reader an idea of the comparisons that are made in this thesis. Finally, and perhaps most importantly, this chapter is intended to give the reader an idea of the context in which this thesis was developed, and its relevance in the field of

thermospheric modelling.

1.1 Nitric Oxide in the lower thermosphere

Nitric Oxide (NO) is a highly variable, key minor constituent in the thermosphere, where it plays an important role in the chemical processes that occur there. The processes in which it takes part has a wide range of effects, which include the formation of the lower ionosphere, the catalytic destruction of ozone and the temperature variations in the thermosphere. These effects of NO have led to considerable interest in studying, observing and modelling it over the years.

In many ways this interest can be traced back to the original proposition by M.Nicolet in 1945, that the ionization of NO by Lyman-α radiation from the Sun played an important role in the formation of the day time ionosphere. NO, having the lowest ionization potential among the neutral constituents present at around 100 km was thought to significantly contribute to formation and chemistry of the D region of the ionosphere. It was also theorized that NO took part in charge transfer reactions with ions to generate NO^+; which in turn produced excited nitrogen atoms ($N(^2D)$) via a dissociative recombination process, which finally completed a loop of reactions by recycling the NO that was originally ionized. This process involving NO^+, $N(^2D)$ & NO is outlined below [3]:

NO contributes to the formation of the D-region of the ionosphere, producing NO^+ by photoionization by the Lyman-α radiation from the sun:

$$NO + hv \rightarrow NO^+ + e \tag{1.1}$$

It is also generated by means of a charge exchange reaction of NO with O_2^+:

$$O_2^+ + NO \rightarrow O_2 + NO^+ \tag{1.2}$$

NO^+ is primarily lost the following reaction:

$$NO^+ + e \rightarrow N(^2D) + O \tag{1.3}$$

$N(^2D)$, an excited state of the nitrogen atom, is produced by the following reactions:

$$N_2^+ + O \rightarrow NO^+ + N(^2D) \tag{1.4}$$

$$N_2^+ + e \rightarrow N(^2D) + N(^4S) \tag{1.5}$$

$$N_2 + e^* \rightarrow N(^2D) + N(^4S) + e \tag{1.6}$$

The first two equations are examples of *dissociative recombination* of the ionized NO and the N_2 molecule, while the latter is the *dissociative excitation* of the nitrogen molecule by photoelectrons.

The realization of the importance of NO in the ionosphere led to the analysis of the production and loss mechanisms of NO, which have been studied and modeled since [4, 5]. It has been shown that the main production mechanisms for NO is the reaction of $N(^2D)$, or $N(^4S)$, a ground state nitrogen atom, with molecular oxygen:

$$N(^2D,^4S) + O_2 \rightarrow NO + O \tag{1.7}$$

The reaction with $N(^2D)$ is the more dominant mechanism at the altitude where NO density is seen to peak, while the reaction with $N(^4S)$ is a strongly temperature dependant reaction and is more important at higher altitudes in the atmosphere.

An important part of this thesis is the contribution of the first excited state of molecular nitrogen, $N_2(A)$ to the production of NO in the thermosphere.

$$N_2(A) + O \rightarrow NO + N(^2D) \tag{1.8}$$

This reaction is important to the chemistry as it generates both a NO and N(^{2}D), the latter of which further contributes to NO production.

Finally, NO is lost in the thermosphere by the following processes:

The reaction with ground state nitrogen atoms:

$$NO + N(^4S) \rightarrow N_2 + O \tag{1.9}$$

Charge exchange with ionized molecular oxygen:

$$NO + O_2^+ \rightarrow NO^+ + O_2 \tag{1.10}$$

And during the daytime, by photodissociation:

$$NO + hv \rightarrow N(^4S) + O \tag{1.11}$$

The importance of the rate co-efficients and the temperature dependence associated with these reactions are shown and discussed later in this thesis.

Apart from playing a role in the formation of the lower ionosphere, NO is known to catalytically react with ozone to produce nitrogen dioxide, which reacts with atomic oxygen to reproduce nitric oxide:

$$NO + O_3 \rightarrow NO_2 + O_2 \tag{1.12}$$

$$NO_2 + O \rightarrow NO + O_2 \tag{1.13}$$

Thus the nitric oxide gets recycled, and it can go on to repeat this process and destroy ozone. This is especially true in the case of polar nights where photodissociation of NO does not occur.

1.2 Thermospheric Modelling of NO

We have seen from the previous section that nitric oxide, a minor neutral species in the field of aeronomy, plays an important role in determining the chemical and physical structure of the thermosphere. Hence it is important to accurately represent NO in an atmospheric model.

TIEGCM, the result of many years of effort at NCAR, had its beginnings in 1981 with the TGCM (Thermospheric General Circulation Model), with the primary impetus being the need to incorporate the effects of thermospheric winds and its coupling with temperature while modelling the structure of the thermosphere. The TGCM evolved to include ionospheric effects (TIGCM) and also electrodynamic interactions between the thermosphere and ionosphere to reach its present form as the TIEGCM. Though used in this thesis to primarily model NO, it also predicts neutral and ion densities in the thermosphere, and can also model thermospheric winds.

The plots included below show a comparison between the modelled and observed NO densities at the equator in the year 1999 for 110 and 150 km. These are the altitudes for the peak NO density and EUV energy deposition respectively. The simulated data used in these plots is from the current version of the TIEGCM without any changes to its chemistry. The comparisons are made at an altitude of 110 km and 150 km. We can immediately see that at 110km the model does a reasonable job of modelling the observed data, while at 150km the errors are more pronounced.

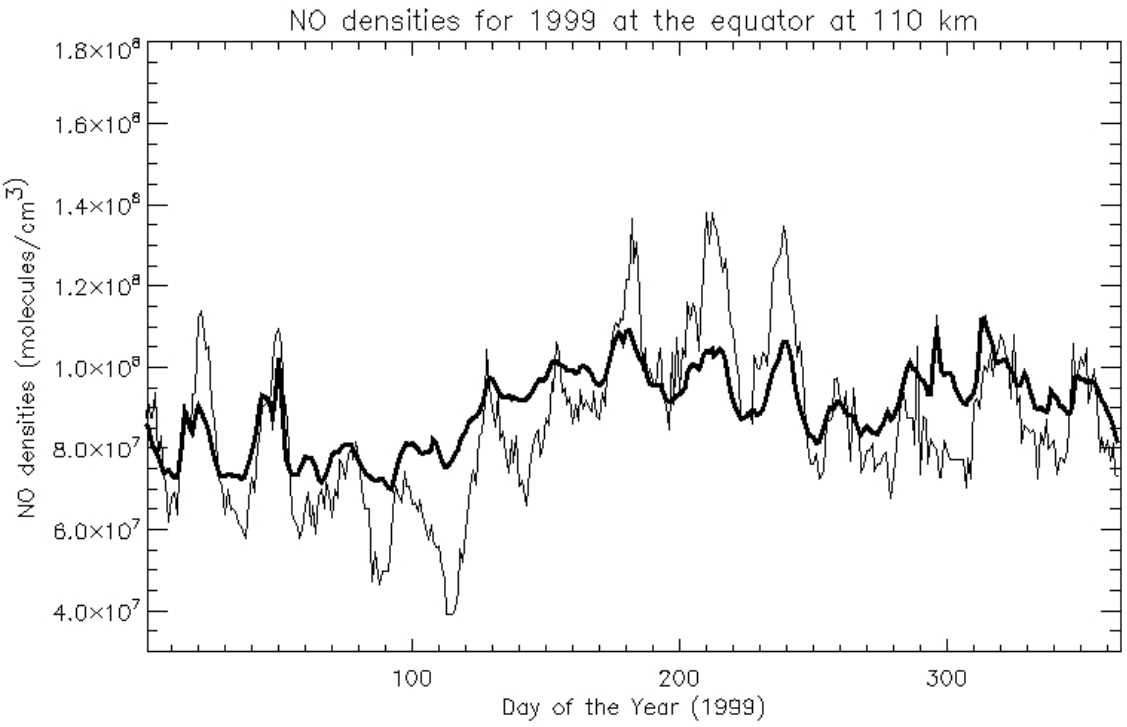

Figure 1.1: NO number densities by SNOE and TIEGCM at 110 km at the equator, 1999.

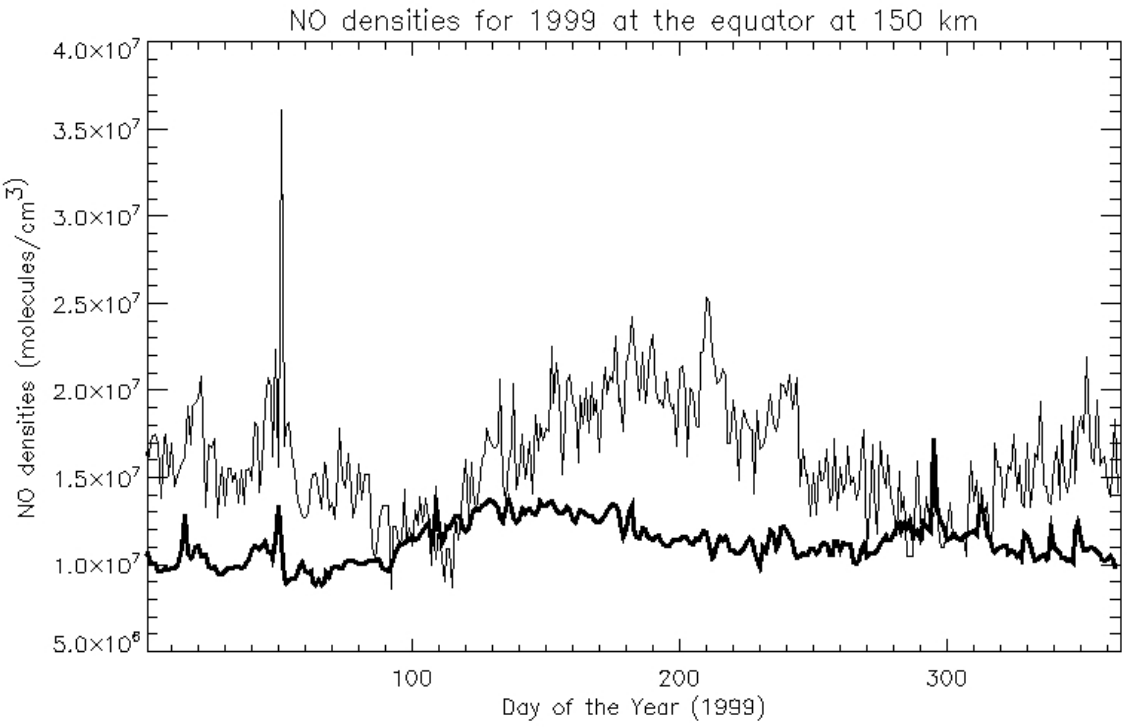

Figure 1.2: NO number densities by SNOE and TIEGCM at 150 km at the equator, 1999.

It is important to emphasize at this point that though the TIEGCM does a seemingly reasonable job of predicting NO densities at 110 and 150 km, the chemistry drving the results are inaccurate. While the basic framework for the calculating NO densities does exist in the model, the results used do not reflect the current understanding of NO production and loss mechanisms. As a result, many modifications made to the model in this thesis are simply updates to the NO chemistry which reflect a more recent understanding of the processes involved. The most important change introduced is that of a NO production mechanism involving the first excited state of molecular nitrogen, $N_2(A)$, which is currently not present in the model. Its reaction with atomic oxygen has been shown to play an important role in the production of NO. Hence, the updated chemistry scheme is introduced into the model in order to represent a more current understanding of the NO chemistry, and to consequently try and improve model-data agreement.

1.3 Overview of Thesis

The remainder of this thesis is organized as follows - Chapter 2 presents the TIEGCM in further detail; we look at the inputs required by the model and the outputs generated by it. Also examined are the initial & boundary conditions and the equations solved by the model. Brief instructions are provided regarding setting up the model and making runs. Chapter 3 considers the changes made to the model as a part of the updated chemistry scheme mentioned previously. The changes made are individually presented, and the rationale behind the changes are briefly explained. The corresponding changes required in the code of the model are also noted in this chapter. Chapter 4 discusses the results of the changes made to the chemistry of the model. We compare the results of the model and the SNOE data at different altitudes for each change, and the updated chemistry scheme as a whole. Finally, Chapter 5 concludes the thesis with a discussion on the updated chemistry scheme and the effect on the model's ability to predict NO densities. The importance of the primary focus of the changes, the $N_2(A)$ chemistry, with regards to the model is noted in this chapter. Future work regarding the TIEGCM and NO modelling is also presented.

Chapter 2

Description of the TIEGCM

This chapter describes the NCAR TIEGCM in further detail - Inputs, boundary conditions, and equations solved by the model are presented.

The TIEGCM is a three dimensional numerical model of the earth's upper atmosphere, with a lower boundary of 97 km and an upper boundary that varies between 500 and 700 km. It solves a self consistent aeronomic scheme of the coupled thermosphere and the ionosphere at every time step, producing a representation of the upper atmosphere's structure in terms of temperatures, winds and densities. Solar EUV flux forms the primary input for the model, while indices such as K_p and $F_{10.7}$ characterize the auroral energies and EUV variability at different wavelengths.

The Thermosphere General Circulation Model (TGCM) and Thermosphere/Ionosphere General Circulation Model (TIGCM) [6], [7] are two general circulation models that were also developed at NCAR, that form the origins of the present day TIEGCM. The TGCM modeled the thermosphere in terms of temperature perturbations and wind structure, primarily by solving the thermodynamic equation and the continuity equation using the assumption of hydrostatic equilibrium. The TIGCM expanded upon this by including a self-consistent aeronomic scheme to compute total temperatures, densities of neutral species such as N(^{4}S),

N(^{2}D) and NO, and calculates a global ionosphere in terms of various ion densities. Building upon this, the TIEGCM included electrodynamic interactions between the thermosphere and the ionsphere and a more realistic non-dipolar geomagnetic field model, allowing calculations of the dynamo effects of thermospheric winds and neutral/plasma dynamics. At present, it is widely used in the atmospheric science community, and represents our best understanding of many aspects of the atmosphere, and specifically, the thermosphere-ionosphere interactions.

2.1 Equations

The equations driving the physics of the aforementioned models are presented below. The primary independent variables in these equations are time (t), latitude (ϕ), longitude (λ) and the model vertical coordinate z, calculated as $log_e(p_0/p)$, where p_0 is the reference pressure and p is pressure. These equations are solved using a finite differencing technique at every timestep.

The Thermodynamic Equation

$$\frac{\partial T}{\partial t} = \frac{ge^z}{p_0 c_p}\frac{\partial}{\partial z}\left(\frac{K_T}{H}\frac{\partial T}{\partial z}\right) - aT - \mathbf{V}.\nabla T - w\left(S + \frac{\partial T}{\partial z} + \frac{RT}{c_p m}\right) + Q'/c_p \qquad (2.1)$$

Which relates the total change in energy with time $\partial T/\partial t$, to the verical conduction, the radiative loss aT, horizontal advection ($\mathbf{V}.\nabla T$), conduction by winds and the heating input Q'/c_p.

The Continuity Equation

$$\frac{1}{rcos\phi}\frac{\partial}{\partial\phi}(vcos\phi) + \frac{1}{rcos\phi}\frac{\partial u}{\partial\lambda} + e^z\frac{\partial}{\partial z}(e^{-z}w) = 0 \qquad (2.2)$$

Which is the usual continuity equation for thermospheric neutral gas, in terms of the eastward, northward and vertical velocities (u,v and w).

The Hydrostatic Equation

$$\frac{\partial \Phi'}{\partial z} = \frac{R(T_0 + T)}{m} \tag{2.3}$$

Which relates the change in the geopotential Φ', with height, to the temperature T and mean molecular mass m. R is the universal gas constant.

The Eastward Momentum Equation

$$\begin{aligned}\frac{\partial u}{\partial t} = \frac{ge^z}{p_0}\frac{\partial}{\partial z}\left(\frac{\mu}{H}\frac{\partial u}{\partial z}\right) + \left(f + \frac{u}{r}tan\phi - \lambda_{xy}\right)v - \lambda_{xx}u - \mathbf{V}.\nabla u - w\frac{\partial u}{\partial z} \\ -\frac{1}{rcos\phi}\frac{\partial \Phi'}{\partial \lambda} + (F_\lambda + \lambda_{xy}v_I + \lambda_{xx}u_I)\end{aligned} \tag{2.4}$$

The Northward Momentum Equation

$$\begin{aligned}\frac{\partial v}{\partial t} = \frac{ge^z}{p_0}\frac{\partial}{\partial z}\left(\frac{\mu}{H}\frac{\partial v}{\partial z}\right) - \left(f + \frac{u}{r}tan\phi - \lambda_{yx}\right)u - \lambda_{yy}v - \mathbf{V}.\nabla v - w\frac{\partial v}{\partial z} \\ -\frac{1}{r}\frac{\partial \Phi'}{\partial \phi} + (F_\phi + \lambda_{yy}v_I + \lambda_{yx}u_I)\end{aligned} \tag{2.5}$$

Where μ is the viscosity coefficient, H is the mean scale height, f is the coriolis parameter, λ is the ion drag tensor, r is the distance from the center of the earth and F_λ and F_ϕ are the zonal and meridional momentum sources. The two equations relate the change in velocities with time $(\partial u/\partial t, \partial v/\partial t)$ with the vertical viscosity term, the coriolis, momentum and ion drag force, horizontal and vertical advection, and the pressure gradient force.

2.2 Inputs

A more comprehensive document covering many aspects of the model not presented here is the TIEGCM model description provided by the HAO. However, presented in this section are a few of the inputs, boundary conditions etc. relevant to the work presented here.

2.2.1 Solar Input

The TIEGCM uses the EUVAC (EUV flux model for Aeronomical Calculations) as the default solar input for the spectral range of 5-105 nm. EUVAC is an empirical representation of the solar irradiance, generated by using a reference spectrum at solar minimum and a wavelength dependent variability depending on solar activity. The variability is characterized by solar indices, most frequently the $F_{10.7}$ index. The EUVAC spectrum is calculated as:

$$f(\lambda) = f_{ref}(\lambda)[1 + A(\lambda)(P - 80)] \tag{2.6}$$

where f_{ref} is the spectrum at solar minimum, A is the wavelength dependent variability factor, and $P = (F_{10.7} + F_{10.7A})/2$. $F_{10.7A}$ is the 81 day average of $F_{10.7}$.

Instead of using a solar proxy model, one can also use measured solar irradiance spectra as an input. An example of this is the TIMED/SEE instrument that captures the solar spectra between 0.1 and 195nm. The data can be processed into a binning scheme compatible with the model and specified in a netCDF file format. If such an input file is provided, the EUVAC model values are overridden.

Example of inputs that are not controlled by the user include the solar flux, ionization branching ratios and cross sections and absorption coefficients. Though these cannot be changed from the input parameter list that the user specifies for a model run, they can be changed from the relevant sub-routines.

2.2.2 Magnetospheric Inputs

High latitude ion convection and the aurora are the two main magnetospheric inputs to the model. The former is done by means of empirical models within the TIEGCM - the Heelis and the Weimer 2005 ion convection models. The **Heelis model** model uses the K_p index, while the Weimer model uses interplanetary magnetic field (IMF), solar wind speed (Vsw)

and solar wind density (Dsw) as inputs. Both the models use this data to compute the cross polar cap potential and hemisphere power which are used in calculating the aurora and auroral radius. The choice of model to be used by the TIEGCM is determined at run time as specified in the input parameter defined by the user. The auroral calculations which determines high latitude energetic particle precipitation can also be turned off from the list.

2.2.3 Boundary Conditions

The TIEGCM has a lower boundary corresponding to a height of approximately 97km, and an upper boundary ranging between 500km and 700km, depending on solar activity. The height of the upper boundary is variable as the TIEGCM uses a constant pressure grid rather than a constant altitude grid for the vertical axis. As a result, the geopotential height of the upper boundary varies with solar activity and its height is calculated at each time step. The height of the lower boundary is also affected by solar activity, but the effect is relatively negligible.

The vertical grid of the model is divided into 29 pressure levels denoted by the variable Z calculated as $log_e(p_0/p)$ ranging from -7 to 7. At the lower boundary of the model, the background thermosphere is specified, over which migrating tidal perturbations due to solar inputs can be added. These perturbations are introduced into the model by using either Hough Modes or the Global Scale Wave Model (GSWM). These tidal perturbations are also used to specify the horizontal velocities and the neutral temperature at the lower boundary. The electron temperature is set to be equal to the neutral temperature.

With regards to chemical species, O_2 is set to a fixed mixing ratio of 0.22, N(^{4}S) and O^+ are in photochemical equilibrium and the vertical gradient of the mixing ratio of O is set to zero.

At the upper boundary, NO and N(^{4}S) are in photochemical equilibrium while the different velocities and the major neutral species (O,O_2 and N_2) are in diffusive equilibrium.

2.3 Outputs

The TIEGCM outputs the following variables in three spatial dimensions over time : height of constant pressure surfaces, neutral, ion and electron temperatures , zonal, meridional and vertical neutral winds, electric potential in geomagnetic/geographic co-ordinates, and the following neutral and ion species - O, O_2, NO, N(^{4}S), N(^{2}D), O^+, N_2^+, NO^+, N^+ and electron density

Chapter 3

Modifying the TIEGCM

This chapter discusses the changes introduced into the NO chemistry scheme contained in the model, and the justification for each change. Also presented are relevant portions of the code from the model and the changes made to them. As mentioned previously, many changes made to the model are simply updates to the existing chemistry reflecting newer results. The emphasis of this chapter however, is on introducing the $N_2(A)$ chemistry which is currently not present in the model. Overall, the changes presented below are part of a revised NO chemistry scheme [8].

The TIEGCM is written in standard FORTRAN-90. As most of the changes presented below simply involve updating rate coefficient values or changing of production/loss rates of species, knowledge of coding in FORTRAN is not strictly required. The existing code in the model tends to serve as a template on which users may base their changes. It is advisable to create a copy of the original source code of the model before proceeding with the changes. The steps involved in running the model itself are not affected by the changes to the code.

The subsections below are grouped together based on the nature of the change and are titled with the chemistry affected rather than the TIEGCM code affected for sake of clarity. Bold text is used either to denote file names or to draw attention towards code snippets, while

emphasis is used for variable names used in the model.

The following are the source files mainly relevant to the changes made here: **comp_n2d.F** which computes N(^{2}D) densities; **comp_n4s.F** the corresponding file for N(^{4}S); **comp_no.F**; **chemrates.F** is the file defining neutral and ion chemistry rates; and **qrj.F** which calculates ionization, dissociation and heating rates along with solar inputs in the model.

3.1 Modified branching ratios

3.1.1 $NO^+ + e \rightarrow 0.95N(^2D) + 0.05N(^4S) + O$

This is the principal production mechanism for N(^{2}D). Though it is known to favor the N(^{2}D) channel more, the branching ratio of 0.85 used in for the channel in the TIEGCM is less than the estimates found in recent studies. More recent data of this branching ratio obtained from Hellberg et al. [9] has shown it to be 0.95 for the N(^{2}D) channel, and correspondingly 0.05 for N(^{4}S).

In the N(^{2}D) and N(^{4}S) computations, the production associated with the rate coefficient $ra1$ and the NO^+ ion density (nop) is multiplied by this branching ratio.

ra1(k,i,lat)*nop(k,i)*{branching ratio}

These branching ratios are changed to 0.95 and 0.05 in **comp_n2d.F** and **comp_n4s.F** respectively.

3.1.2 $N_2^+ + e \rightarrow 1.52N(^2D) + 0.48N(^4S)$

At altitudes below 150 km, the reaction with atomic oxygen to produce NO^+ is the dominant loss mechanism for N_2^+. Hence this dissociative recombination reaction, while not an important source for NO production, is still a source for N(^{2}D) and N(^{4}S) and is changed

here to reflect a more accurate value for the branching ratio. The branching ratios were shown to be 1.52 and 0.48 respectively by Peterson, et al. [10]. The branching ratios used previously in the model are 0.9 and 1.1.
The term associated with this reaction, found in **comp_n2d.F** and **comp_n4s.F** is:

ra3(k,i,lat)*n2p(k,i)*{branching ratio}

3.1.3 $N_2 + hv/e^* \rightarrow 0.5N(^2D) + 0.5N(^4S)$

The branching ratio for dissociation of nitrogen by electron impact and EUV photoabsorption to produce N(^{2}D) is denoted by the variable *brn2d* in the TIEGCM. (1-*brn2d*) hence gives the branching ratio for N(^{4}S). Values for this parameter ranging from 0.75 to 0.5 can be found in the literature [11][5][12], indicating the uncertainties associated with this term. However, we use a N(^{2}D) yield of 0.5 as obtained by Zipf et al. [11].

As shown by Barth [5] and noted by Yonker et al., [8], the reduction in the branching ratio from 0.6 to 0.5 results in a substantial decrease in NO density, but this should not be attributed to a decrease in efficiency of NO production due to less N(^{2}D) being present; rather the corresponding increase in N(^{4}S) production is what causes to NO to be destroyed more efficiently.

In the TIEGCM, *brn2d* is changed from 0.6 to 0.5 in the **cons.F** file where it is defined at **L.40**.

3.2 Modified rate coefficients

3.2.1 $N(^4S) + NO \rightarrow N_2 + O$

The reaction of NO with N(^{4}S) is the primary loss mechanism for NO in the thermosphere. The associated rate coefficient is crucial to determine the rate of NO loss to N(^{4}S) at both 110

and 150 km. The plot below shows a comparison of the original TIEGCM rate coefficient, along with the theoretical and recommended rates observed for this reaction. At both 110 km and 150 km, where the neutral temperatures are roughly around 300K and 700 K, we see that the TIEGCM uses a higher rate coefficient, i.e, predicts a faster loss of NO to N(^4S). We the JPL recommended rate proposed by Sander et al., [13] and change the temperature dependence of this reaction.

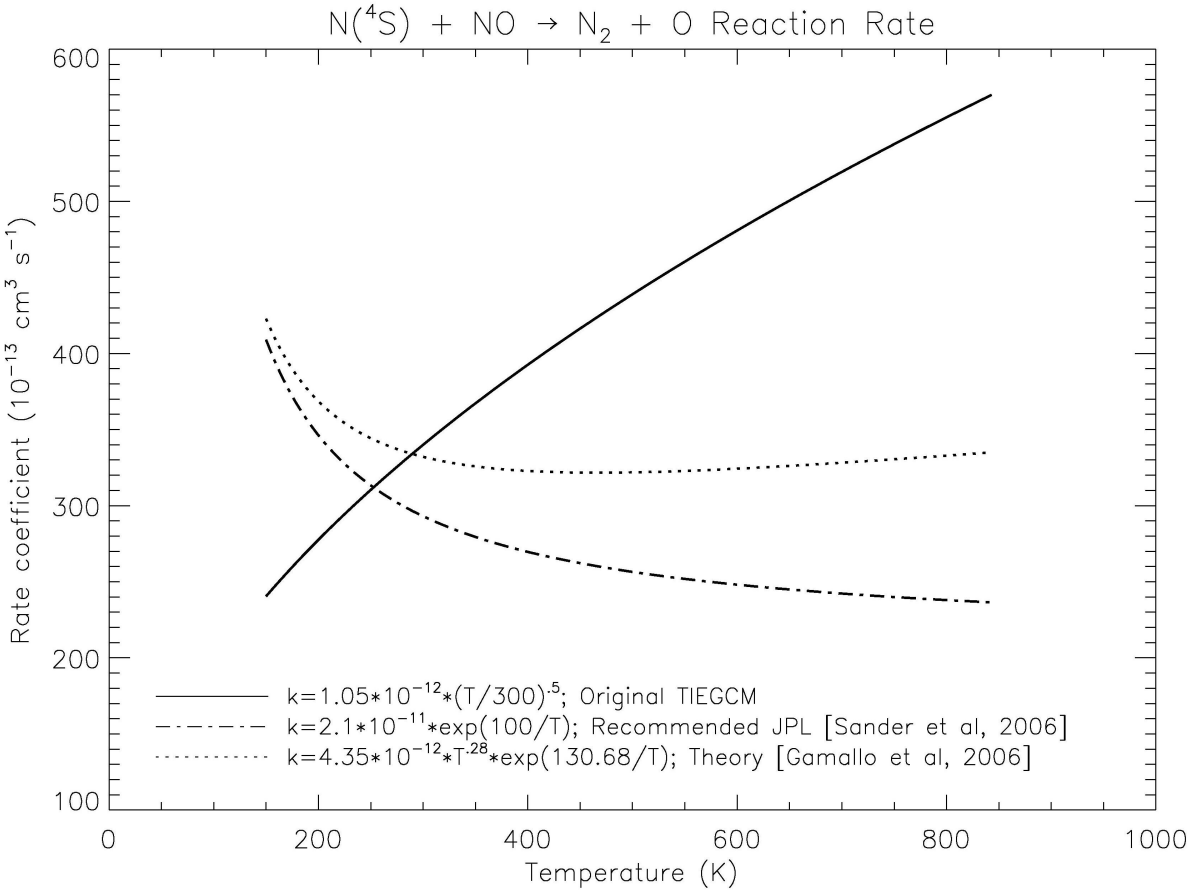

Figure 3.1: Reaction rates for $N(^4S) + NO \rightarrow N_2 + O$

The temperature dependence is changed in **chemrates.F**. It is changed from $beta3 = 3.4\text{x}10^{-11}\sqrt{TN/300}$ cm^{-3}s^{-1} to $2.1\text{x}10^{-11} * e^{100/TN}$ cm^{-3}s^{-1}. This requires changing the expression for $beta3$ on **L.257** of the unmodified code.

3.2.2 $N(^2D) + O_2 \rightarrow NO + O$

This is the main production mechanism of NO from $N(^2D)$. The below plot shows that TIEGCM uses a constant rate coefficient, where as studies have shown a strong temperature dependence of this reaction [14][15]. We use the recommended temperature dependence proposed by Herron, et al. [14]. By an informal inspection of the rate coefficients we can expect an increase in the calculated NO densities at both 110 km and 150 km.

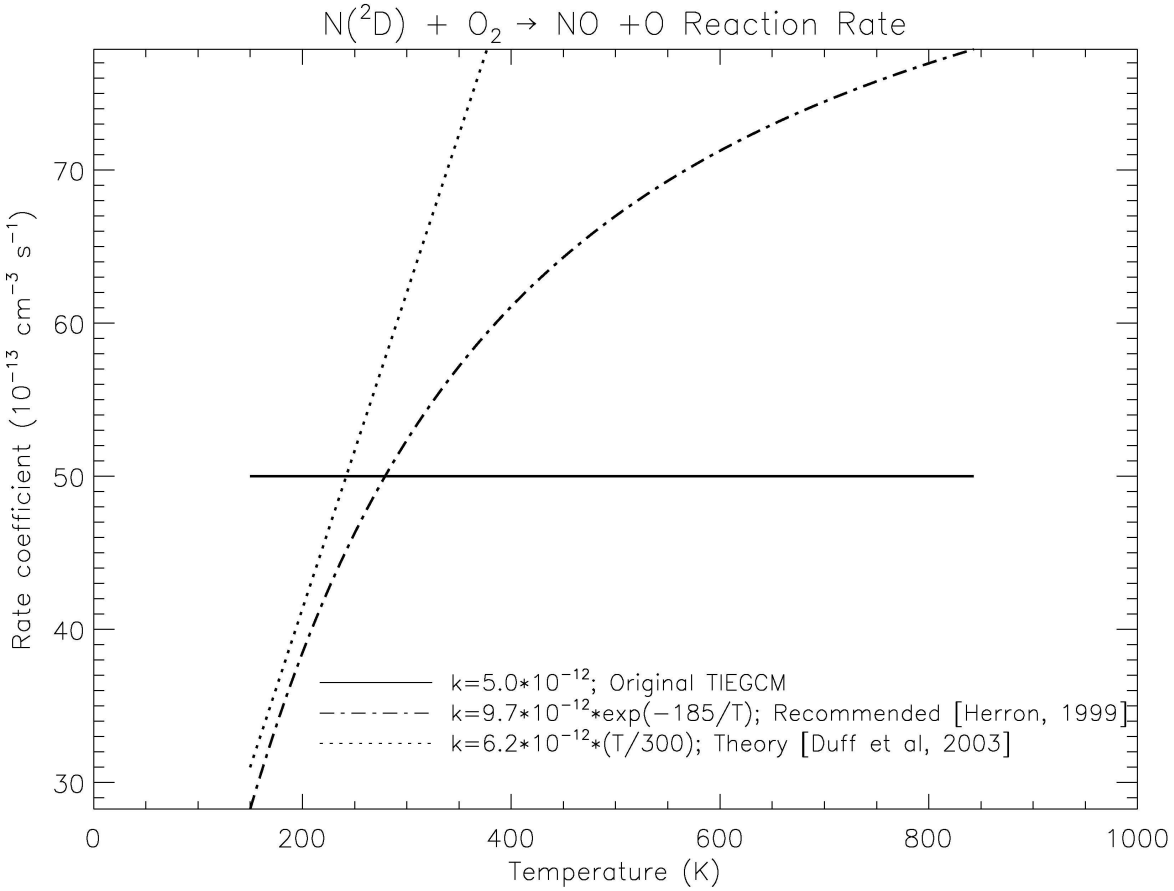

Figure 3.2: Reaction rates for $N(^2D) + O_2 \rightarrow NO + O$

The relevant rate coefficient variable is *beta*2 in **chemrates.F**. It's definition on **L.47** is commented out and is initialized along with the other temperature dependent rates, $beta1 - beta17$. In order to allocate memory to the array corresponding to *beta*2, we use the

following code:

allocate(beta3(nlevp1,lon0:lon1,lat0:lat1),stat=istat)
if (istat /= 0) write(6,"('>>> alloc_tdep: error allocating',
| ' beta3: stat=',i3)") istat

3.2.3 $N(^2D) + O \rightarrow N(^4S) + O$

This reaction is important to NO densities as it removes $N(^2D)$ (which contributes to NO production) and produces $N(^4S)$ (which contributes to NO loss). In the plot below, we see again that the TIEGCM uses a constant rate co-efficient, which is below the recommended and theoretical values at the altitudes of interest. We can hence predict this reaction to reduce NO densities at both altitudes. We introduce the temperature dependence recommended by Yonker et al.[8]

This change is similar to the one made for *beta*2. A temperature dependence is introduced for the neutral rate *beta*4 initially with a value of $7.0\text{x}10^{-13}\text{cm}^{-3}\text{s}^{-1}$ is changed to the equation $beta4 = 1.65\text{x}10^{-12} * \sqrt{TN/260}\text{cm}^{-3}\text{s}^{-1}$. The changes are made to the **chemrates.F** file, and the steps followed are the same as before.

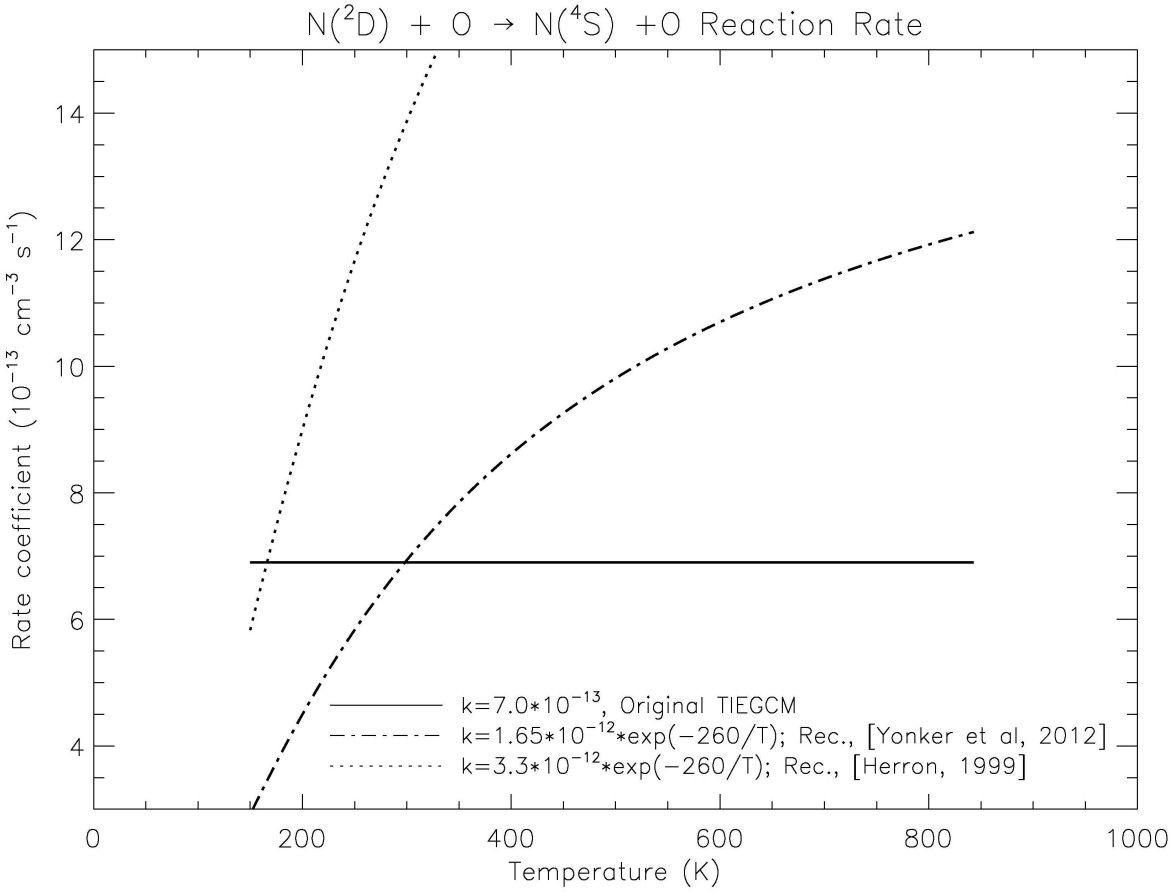

Figure 3.3: Reactions rates for $N(^2D) + O \rightarrow N(^4S) + O$

3.3 Other changes

3.3.1 $\mathbf{N^+ + O_2 \rightarrow N(^2D) + O_2^+}$

In TIEGCM, the above reaction is a production mechanism for N(^{4}S). However, recent work by Midey et al.[16] suggests that that this reaction strongly favors production of N(^{2}D) over N(^{4}S). We hence remove this production mechanism for N(^{4}S) and use it in the N(^{2}D) production calculations. In other words, we change the product of the reaction from N(^{4}S) to N(^{2}D).

The rate coefficient associated with this reaction is the rate coefficient $rk6$, defined in the **chemrates.F** file. The value of this rate is changed to $2\text{x}10^{-6}\text{cm}^{-3}\text{s}^{-1}$ for N(^{2}D) production. We remove the production term for N(^{4}s) in **comp_n4s.F** by removing the term "$rk6 * nplus(k,i) * o2(k,i) * rmassinv\_o2$". This term is then used in **comp_n2d.F** so as to contribute to the total production of N(^{2}D).

The N^+ ion densities ($nplus$) required in the above computation need to be passed to **comp_n2d.F**, hence we add it to the list of variables in the subroutine definition at the top of this file:

subroutine comp_n2d(o2,o1,no,n4s,ne,op,...n2p,nplus ...)

And also define it in the list of input arrays to the subroutine:

real,dimension(lev0:lev1,lon0-2:lon1+2),intent(in) ::
...
| n2p, ! N2+ ion
| nplus, ! N+ ion
| nop, ! NO+ ion
... Lastly, we change the calling definition of this subroutine in **dynamics.F** :
call comp_n2d(
...
| n2p, ! N2+ ion
| nplus, ! N+ ion
| nop, ! NO+ ion
... It should be noted that the order of the variables used in the subroutine definition in **comp_n2d.F** must be maintained in the subroutine call in **dynamics.F**

3.3.2 $N(^2D) + N_2 \rightarrow N(^4S) + N_2$

This loss mechanism for $N(^2D)$ does not currently exist in the model, but has been shown to exist by Herron[14]. Though more than one temperature dependence has been formulated for this reaction, a constant rate coefficient is recommended in the study and is used presently.

A new neutral rate coefficient variable, *beta*18 is defined in **chemrates.F** with a value of $1.7x10^{-14}cm^{-3}s^{-1}$ for this purpose. The variable is declared along with the other constant, neutral chemistry rates at **L.47**. *beta*18 is then included in both **comp_n2d.F** and **comp_n4S.F** as one of the variables called from the **chemrates** module. The following term is then added to the $N(^2D)$ loss and $N(^4S)$ production calculation.

beta18*xn2(k,i)*rmassinv_n2

3.4 $N_2(A)$ Chemistry

The changes required for the $N_2(A)$ chemistry are slightly more extended than the changes above, hence we only provide an outline of the steps here explaining the procedure followed in introducing $N_2(A)$ into the model and using it to compute it. The names of the relevant source files are still provided.

$N_2(A)$ is the first excited electronic state of molecular nitrogen, produced primarily by photoexcitation or decay from higher energy states of the molecule. It is a channel for NO production in the following reaction:

$$N_2(A) + O \rightarrow NO + N(^2D) \tag{3.1}$$

We include this reaction in the TIEGCM chemistry scheme as it has been shown to be important to the NO chemistry and also increases the peak NO density at 110 km by a

factor of 2-3 [17] [18]. It is essential to the present chemistry scheme as it compensates for the reduction in NO densities produced by the change in the branching ratio of photodissociation of N_2, mentioned in section 3.1.3. We compute the N_2(A) production rate by a Gaussian scaling in altitude the production rate of N_2^+ by photoelectron impact. The photoelectron ionization rates are provided in the file **qrj.F**. However, the photoelectron impact ionization rate of N_2 is not directly available in the model. For this, we first define a frequency *qn2pe* which is the ionization rate of N_2 only by photoelectrons. However, this frequency includes both the dissociative and non-dissociative ionization rates. As we are interested only in the latter, we also create a frequency *di_n2e* which is the dissociative ionization of N_2 by photoelectrons. We subtract this from *qn2pe* to obtain the non-dissociative photoelectron ionization rate of N_2. This is generated in **qrj.F** and is passed to the modules where N_2(A) densities are calculated.

As mentioned above, we scale the N_2(A) production rate to the N_2^+ rate, which in turn depends on the mass mixing ratio or partial pressure of N_2. We approximate the scaling in altitude using a linear fit, and as seen from the figures below, this approximation for the N_2 mixing ratios is a very good one over the altitude range where the contribution of N_2(A) is the most significant. The linear scaling is further justified by the fact that the variation in N_2 partial pressure is within a few percent throughout the course of the year, as shown below.

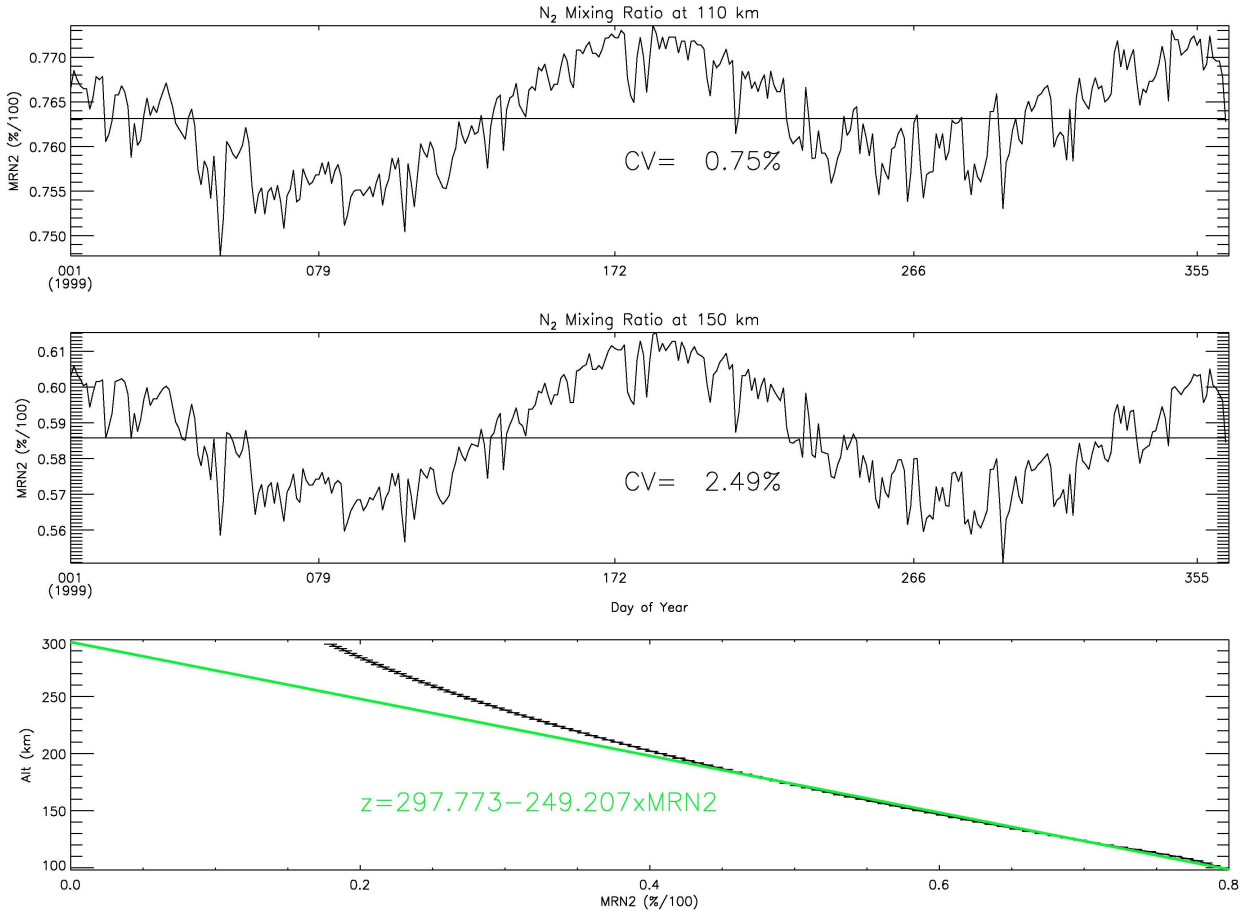

Figure 3.4: N_2 mass mixing ratios at 110 km & 150 km v/s time, and the linear fit used for scaling the N_2^+ production rate to the $N_2(A)$ production

3.5 Summary

The following table summarizes the changes that have been introduced to the model in this chapter.

Table 3.1: Current TIEGCM Modifications

Code	Description	Change	Reference
`ra1`	higher N(^{2}D) yield	$NO^+ + e \rightarrow .95N(^2D) + .05N(^4S) + O$	*Hellberg (2003)*
`ra3`	higher N(^{2}D) yield	$N_2^+ + e \rightarrow 1.52N(^2D) + .48N(^4S)$	*Peterson (1998)*
`brn2d`	lower N(^{2}D) yield	$N_2 + hv/e^* \rightarrow .5N(^2D) + .5N(^4S)$	*Zipf (1978)*
`beta2`	changed TD	$N(^4S) + NO \rightarrow N_2 + O$	*Sander (2006)*
`beta3`	added TD	$N(^2D) + O_2 \rightarrow NO + O_2$	*Duff (2003)*
`beta4`	Added TD	$N(^2D) + O \rightarrow N(^4S) + O$	*Yonker(2011)*
`rk6`	higher N(^{2}D) yield	$N^+ + O_2 \rightarrow N(^2D) + O_2^+$	*Midey (2006)*
`beta18`	new	$N(^2D) + N_2 \rightarrow N(^4S) + N_2$	*Herron (1999)*
`beta19-21`	new	$N_2(A) + O \rightarrow NO + N(^2D)$	*Thomas(1997)*

Chapter 4

Results

In this chapter, we begin by briefly describing the SNOE satellite mission and the observations made. We then proceed to compare the results obtained from the model with the SNOE data.

4.1 SNOE

The Student Nitric Oxide Explorer was designed and built at Laboratory for Atmospheric and Space Physics (LASP) at the University of Colorado, Boulder. The aim of the mission was to analyze the effect of solar and magnetospheric inputs on NO chemistry and density in the lower thermosphere.

The satellite was launched in a sun synchronous orbit with a mean local time of 11 am at equatorial crossing on the day side of the earth. A limb scanning technique was used to measure fluorescent scattering of solar radiation by NO at the wavelengths of 215 and 237 nm using a UV spectrometer. The SNOE data used in this thesis corresponds to the daily average of measurements from 15 orbits of the satellite for the year 1999. The NO densities obtained from TIEGCM corresponds to values taken at a longitude where the solar local

time is 11 am.

SNOE made global observations of Nitric Oxide in the lower thermosphere between February 1998 and December 2003. The year 1999 was chosen for this study as it is the only year with nearly uninterrupted observations of NO. It is worth noting that this year was just prior to the solar cycle maximum, resulting in strong solar activity variations throughout the year. The variation of NO density with sun spots and the rotation of the sun are hence easily observed in the SNOE data.

4.2 Overview of the chemistry

A useful way to look at the thermosphere is to assume a constant background atmosphere comprising of N_2, O_2 and O, and a constantly varying portion comprising of minor species such as NO, N(^{4}S), N(^{2}D), O^+ and NO^+ that react both among themselves and the background atmosphere. The rate of production or destruction of any given species is dictated primarily by the availability of the reactants involved and the rate co-efficient of the reaction. This is important as it dictates which reaction will occur for a given species, at a given altitude, from a set of possibilities. For example, N(^{2}D) may participate in the destruction of NO in a manner similar to N(^{4}S), however the densities of O_2 being larger than that of NO at both 110 and 150 km prevent this from occuring. Also, the temperature dependence of the involved rate co-efficients determines the effect of altitude on these reactions.

The general rule of the thumb with regards to NO chemistry is that more N(^{2}D) equates to more NO. The abundance of O_2 ensures that N(^{2}D) will almost always react with it to produce NO. However, even though the rate coefficient is an increasing expontential with temperature, the reaction becomes less effective at producing NO with increasing altitude as O_2 densities fall away and N(^{2}D) is quenched by atomic oxygen to produce N(^{4}S).

On the other hand, *more* N(^{4}S) equates to *less* NO at lower altitudes. It reacts with NO to produce relatively chemically inert N_2 along with atomic oxygen, and forms the primary

source of NO loss at 110 km. The reaction however has a rate coefficient that is a decaying exponential with temperature, which means that N(^{4}S) becomes less effective at higher temperatures (altitudes) in destroying NO. At 150 km, where the neutral temperatures are higher, N(^{4}S) in fact behaves similar to N(^{2}DS) in that it can contribute to NO production vy reacting with O_2

It is important to understand that there are competing mechanisms involved in the production and loss of NO, N(^{2}D), N(^{4}S), O_2^+ and NO^+ which are all interlinked. It is a complex dance where more often that not the subtle effects of the ratio of concentration of species competing rate coefficients may trip up one's intuition about the effects of changes to the chemistry.

4.3 Model-Data Comparisons

The below plots show the effect of the chemistry scheme introduced to the model. The model runs were made for first 31 days of 1999, and are indicative of the effect of the change introduced to the model, i.e, a similar effect in the NO densities would be seen in the model were to be run for the entire year. Model runs were made to determine the effect of each individual change, followed by a final run with the all the changes proposed in the chemistry scheme.

In the plots below, the thin solid line represents the SNOE data, the thick solid line represents the unmodified TIEGCM, and the dashed line represents the TIEGCM with the change mentioned in the caption. The plots are made at 110 km (NO density peak) and 150 km (EUV energy deposition peak).

Modified branching ratios

These changes are straightforward in that we increase the either production channel of N(^{2}D) or N(^{4}S) in a reaction at the cost of the other. The effect of each individual change is explained below.

4.3.1 $NO^+ + e \rightarrow 0.95N(^2D) + 0.05N(^4S) + O$

Apart from the photodissociation of the nitrogen molecule, this reaction is the most important source of excited and ground state nitrogen atoms. The reduction of N(^{4}S) production reduces the amount of NO that is lost to it, and as we also increase the amount of N(^{2}D) present, we see an overall increase in NO densities at 110 km.

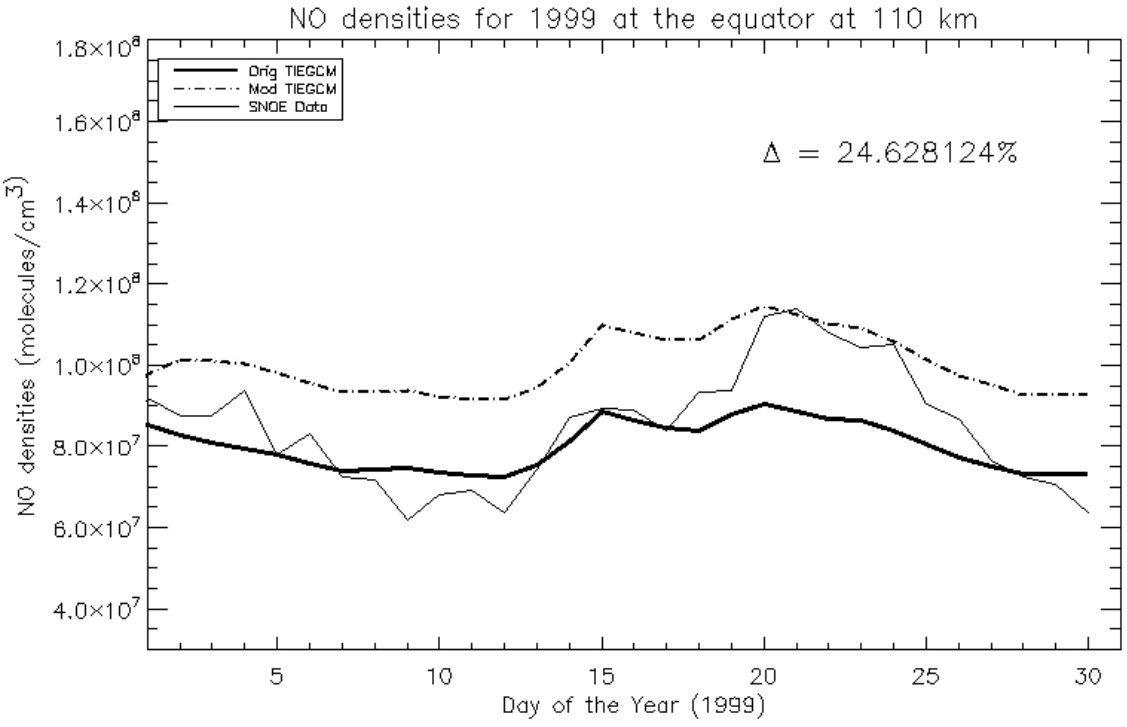

Figure 4.1: Modified branching ratio for $ra1$, effect at 110 km

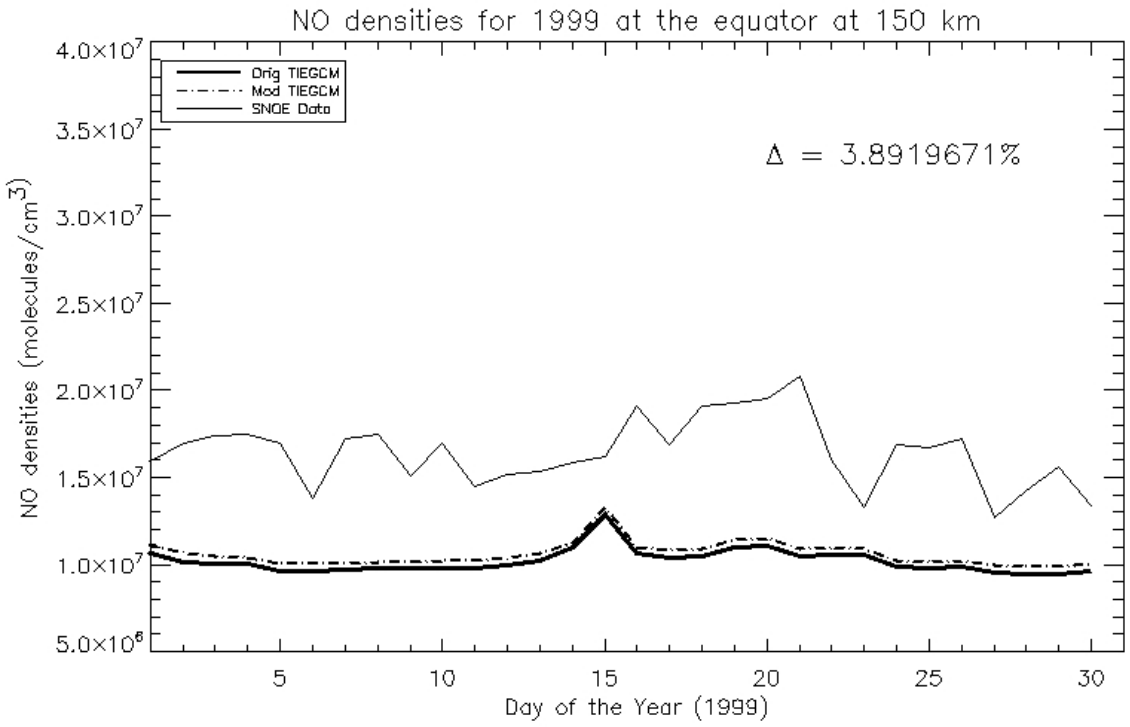

Figure 4.2: Modified branching ratio for $ra1$, effect at 150 km

The fact that the increase of NO densities at 150 km is not as pronounced as seen at 110 km can be attributed to the fact that 150 km there is more atomic oxygen than molecular oxygen - the O_2/O ratio decreases with altitude. As a result, $N(^2D)$ tends to get quenched by atomic oxygen than react with molecular oxygen to produce NO.

4.3.2 $N_2^+ + e \rightarrow 1.52N(^2D) + 0.48N(^4S)$

As mentioned in the previous chapter, this reaction is a comparatively minor contributor to NO densities as the reaction with O to produce NO^+ and $N(^2D)$ is the prevalent reaction below 150 km for N_2^+. The change in the branching ratio was primarily done to reflect newer values obtained from Peterson, et al. [10]. The increase in NO densities seen at both altitudes from this change is an extremely minor one.

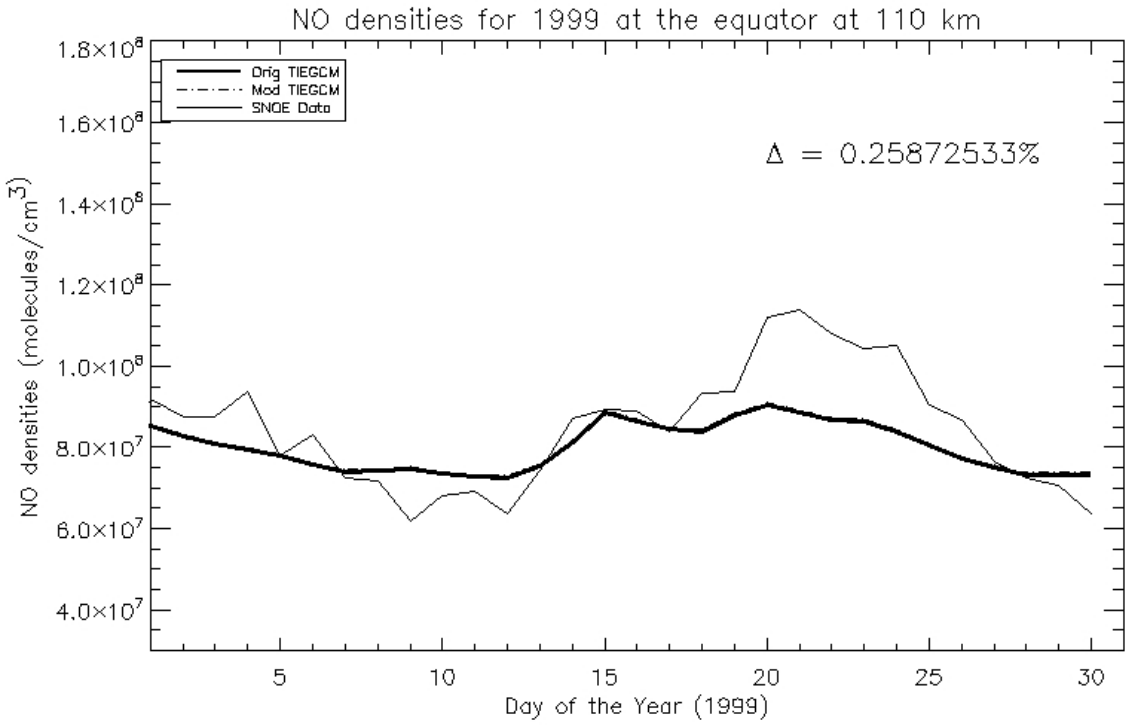

Figure 4.3: Modified branching ratio for $ra3$, effect at 110 km

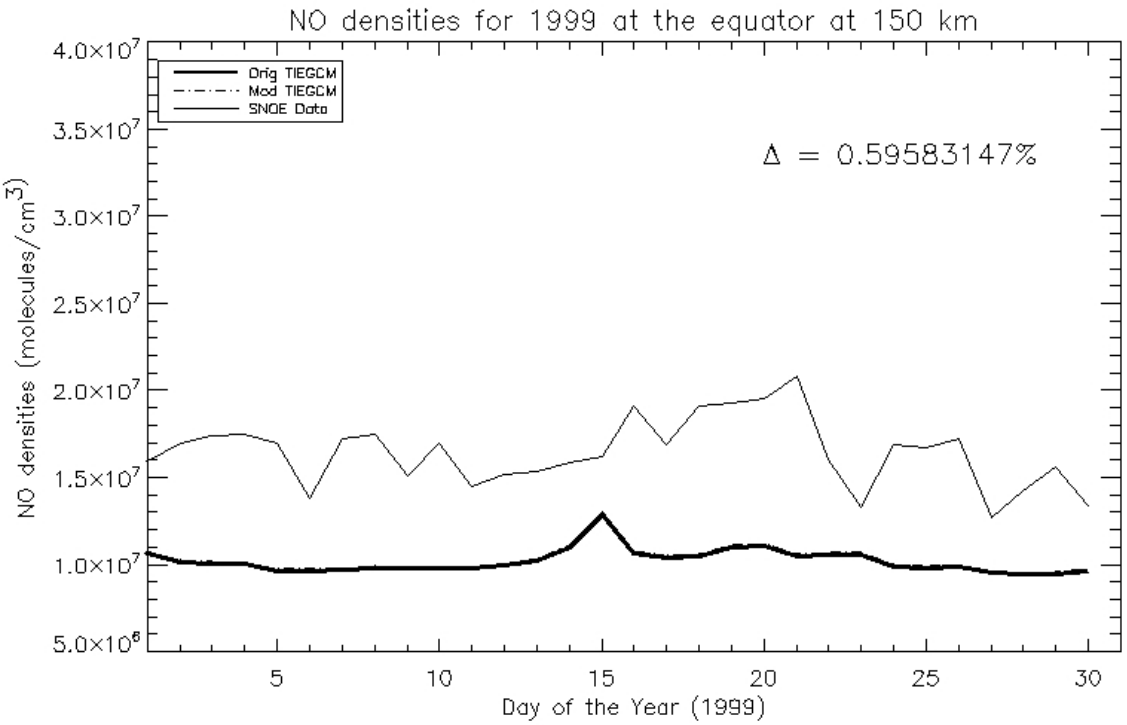

Figure 4.4: Modified branching ratio for $ra1$, effect at 150 km

4.3.3 $N_2 + hv/e^* \rightarrow 0.5N(^2D) + 0.5N(^4S)$

An 80% reduction in NO densities was seen at 105 km when the branching ratio for $N(^2D)$ produced from photodissociation of N_2 was changed from 0.6 to 0.5 [5], using a 1-D NO model. We see a substantial decrease in NO production at 110 km, but not to the same extent.

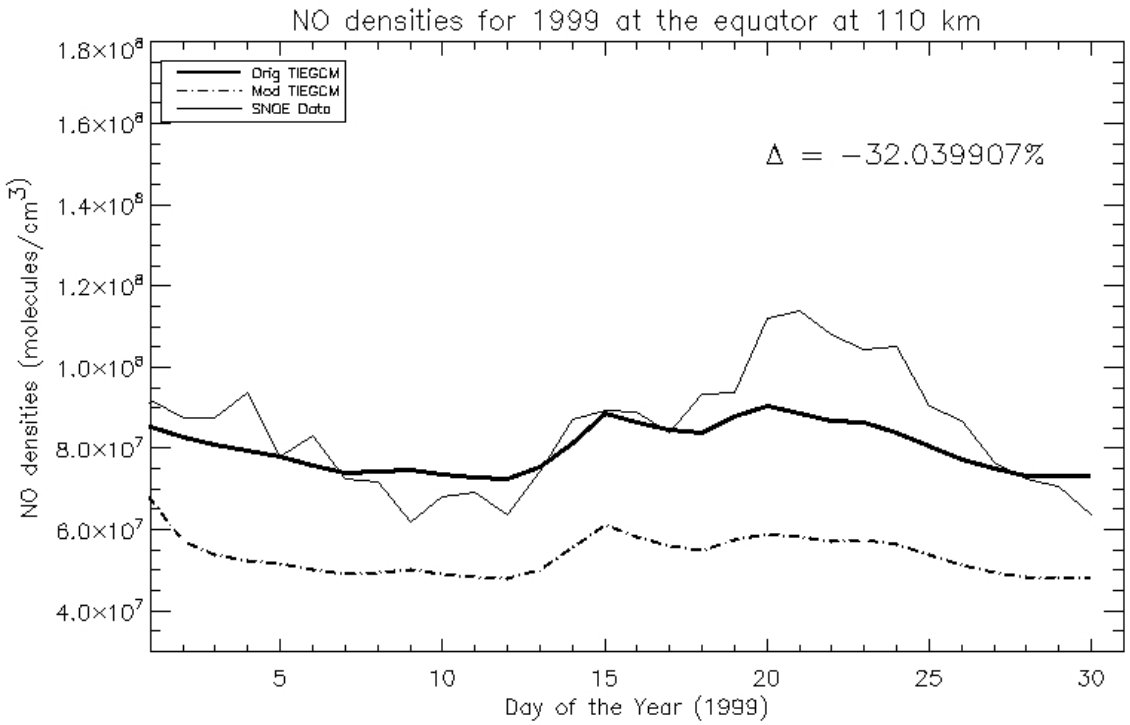

Figure 4.5: Modified branching ratio $brn2d$, effect at 110 km

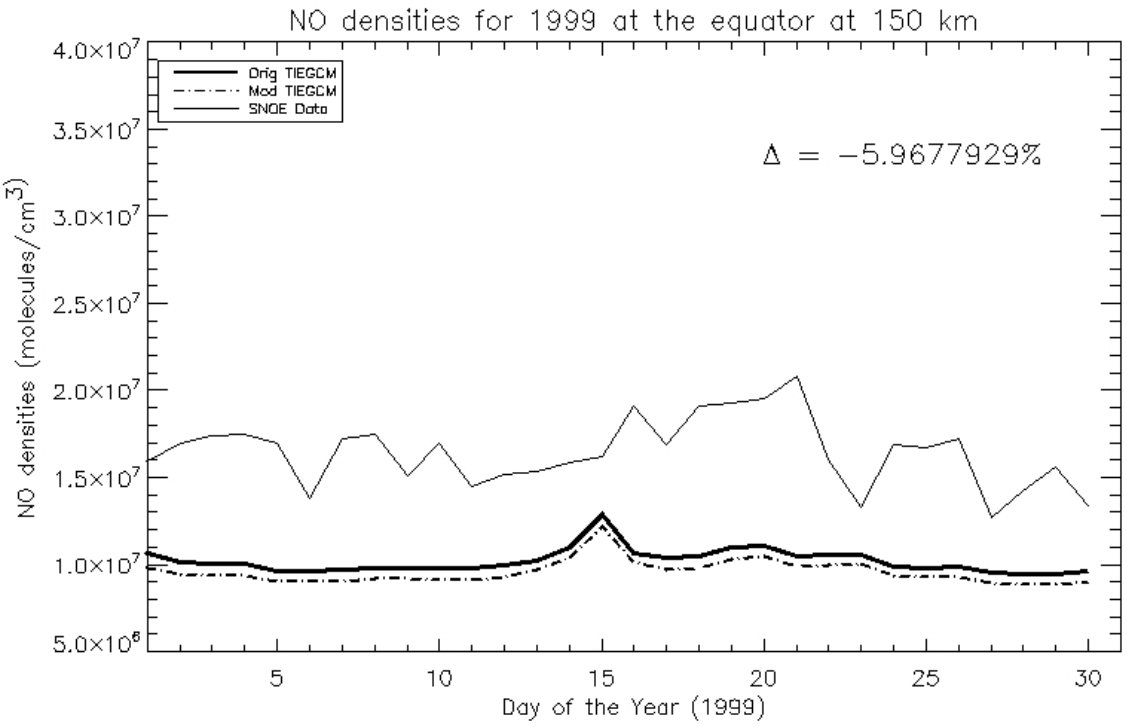

Figure 4.6: Modified branching ratio $brn2d$, effect at 150 km

Changed rate coefficients

4.3.4 $N(^4S) + NO \rightarrow N_2 + O$

As noted before, this reaction is the primary loss mechanism for NO. The reduced rate coefficient for this reaction results in a longer lifetime of $N(^4S)$ at both 110 and 150 km as compared to the original value used in the TIEGCM. As a result, we increase the NO lifetime as well, resulting in increased NO densities.

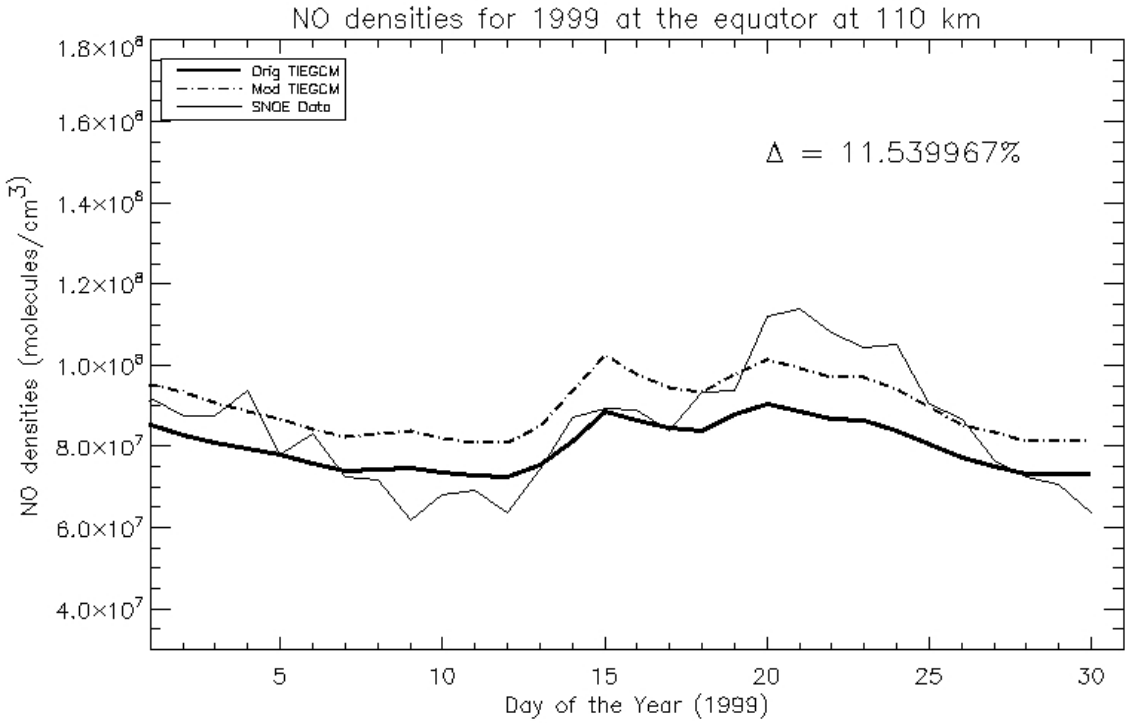

Figure 4.7: Changed temperature dependence of reaction rate *beta*3, effect at 110 km

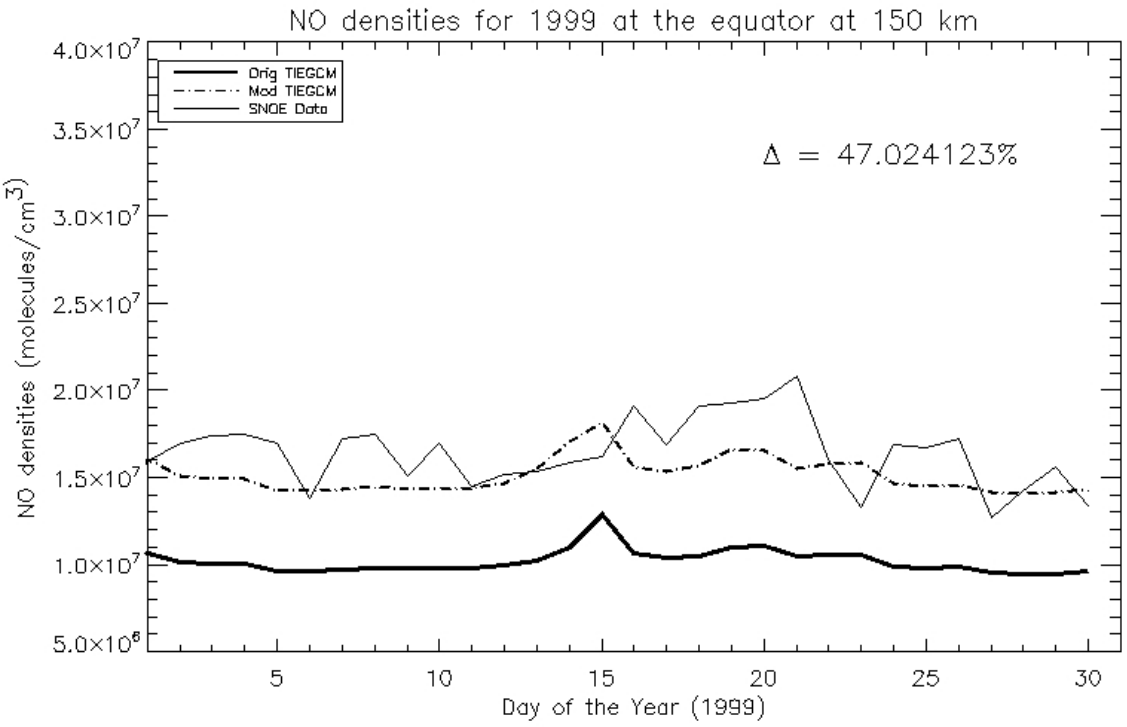

Figure 4.8: Changed temperature dependence of reaction rate *beta*3, effect at 150 km

It is interesting to observe at 150 km that reduction of the rate coefficient for the above reaction results in much larger increase in NO densities that at 110 km. This is because the competing reaction that involves N(^{4}S) loss results in more NO - the reaction is that with O_2. Decreasing the rate coefficient of the above reaction with NO allows more N(^{4}S) to react with O_2 - and both these factors contribute to the large increase in NO densities.

4.3.5 $N(^2D) + O_2 \rightarrow NO + O$

Similarly, increasing the rate coefficient for the above reaction results in $N(^2D)$ reacting faster with O_2 to produce more NO at both altitudes, i.e., a greater NO production rate.

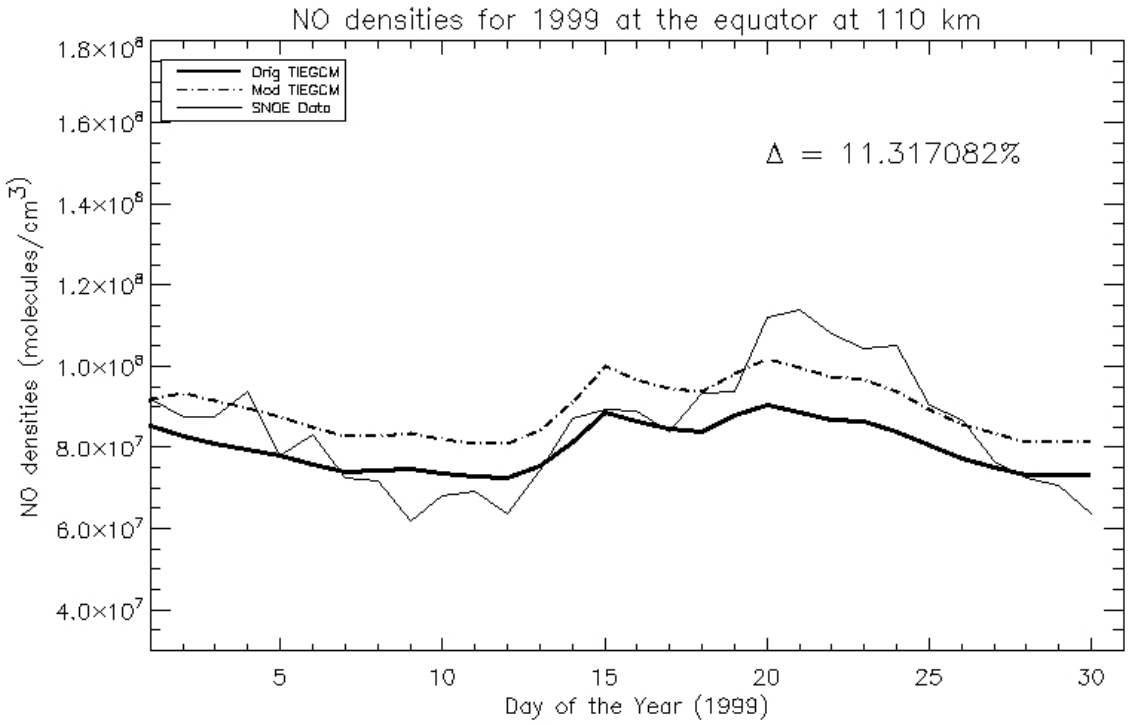

Figure 4.9: Added temperature dependence of reaction rate *beta*2, effect at 110 km

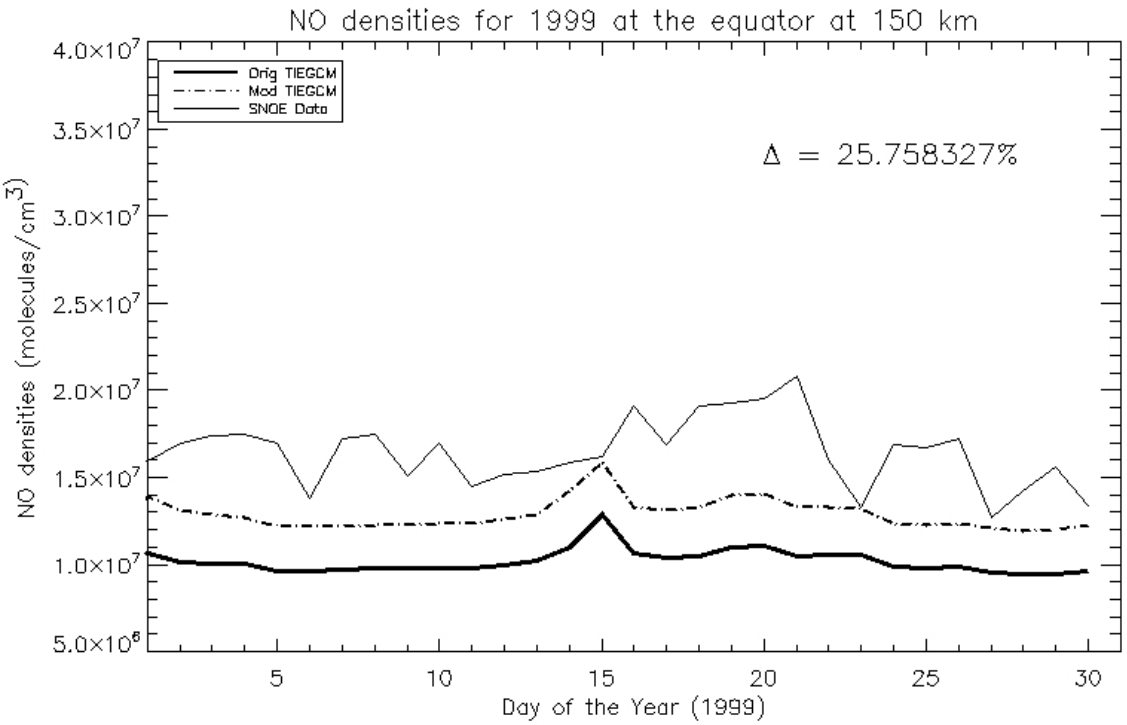

Figure 4.10: Added temperature dependence of reaction rate *beta*2, effect at 150 km

4.3.6 $N(^2D) + O \rightarrow N(^4S) + O$

By increasing the rate at which $N(^2D)$ is lost to O to produce $N(^4S)$, we increase the rate at which NO is lost at 110 km. The rate coefficient is increased from the previous value of $7x10^{-13}cm^{-3}s^{-1}$ both at 110 km and 150 km. However, at 150 km the increase in $N(^4S)$ does not substantially decrease NO densities, as at this altitude it tends to contribute to NO production by reacting with molecular oxygen.

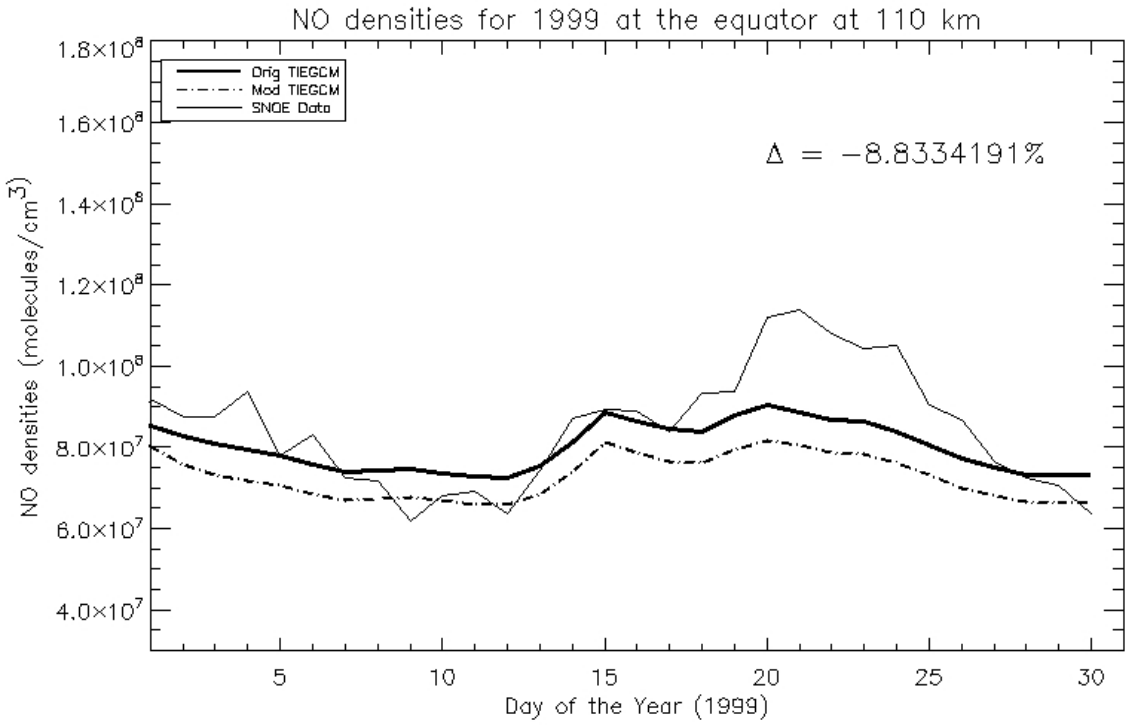

Figure 4.11: Added temperature dependence of reaction rate *beta*4, effect at 110 km

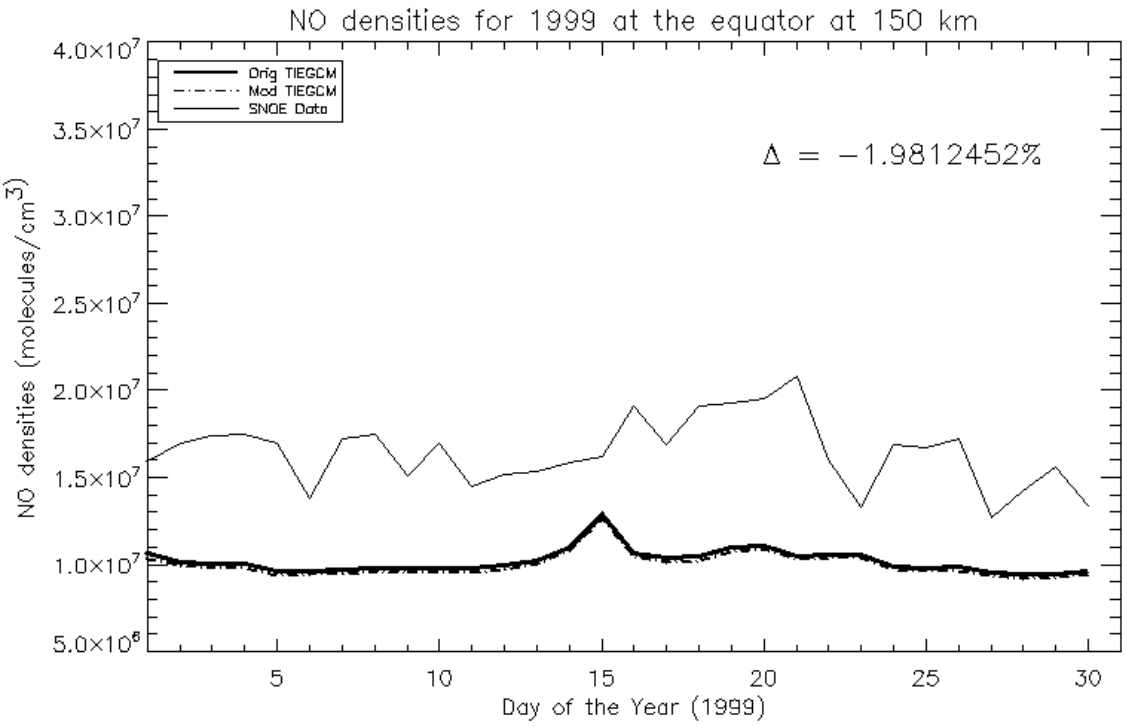

Figure 4.12: Added temperature dependence of reaction rate *beta*4, effect at 150 km

Other changes

4.3.7 $N^+ + O_2 \rightarrow N(^2D) + O_2^+$

This change resulted in changing the product of the above reaction from N(^{4}S) to N(^{2}D). In other words, remove a loss mechanism while also introducing a production mechanism for NO at 110 km. Hence we see that at 110 km the NO densities are increased substantially. We can also infer that this process does not contribute to NO production substantially at 150 km because the N(^{4}S) previously being produced by this reaction was also contributing to NO production.

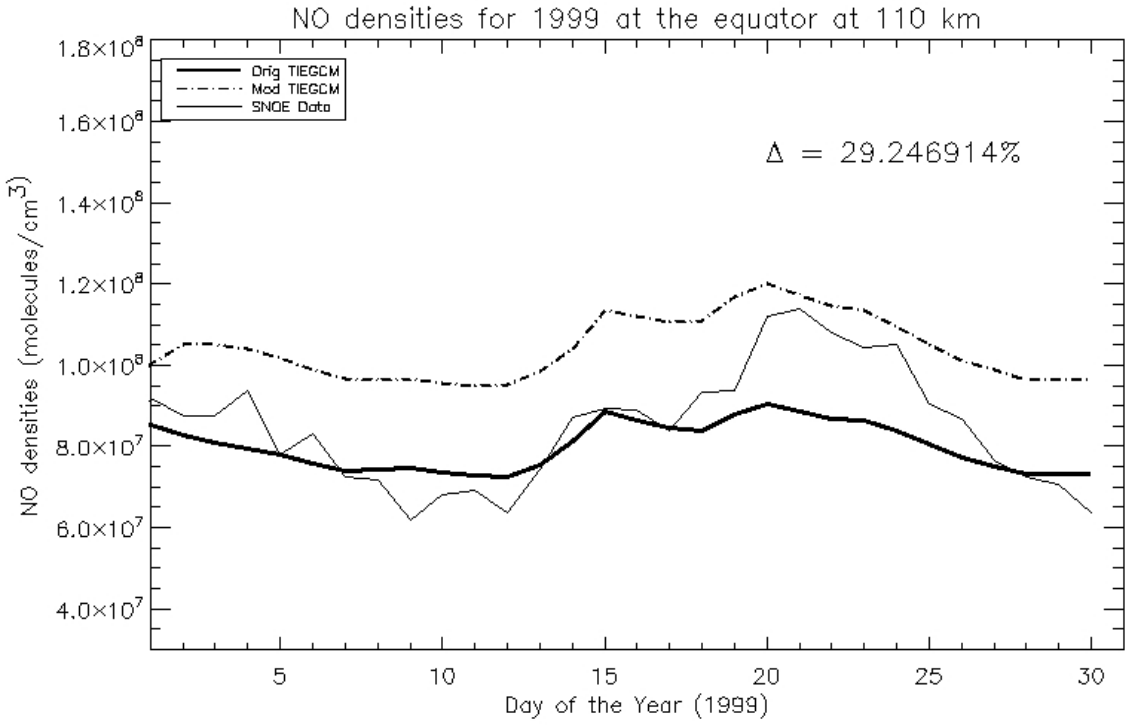

Figure 4.13: $N^+ + O_2 \rightarrow N(^2D) + O_2^+$, increased $N(^2D)$ yield

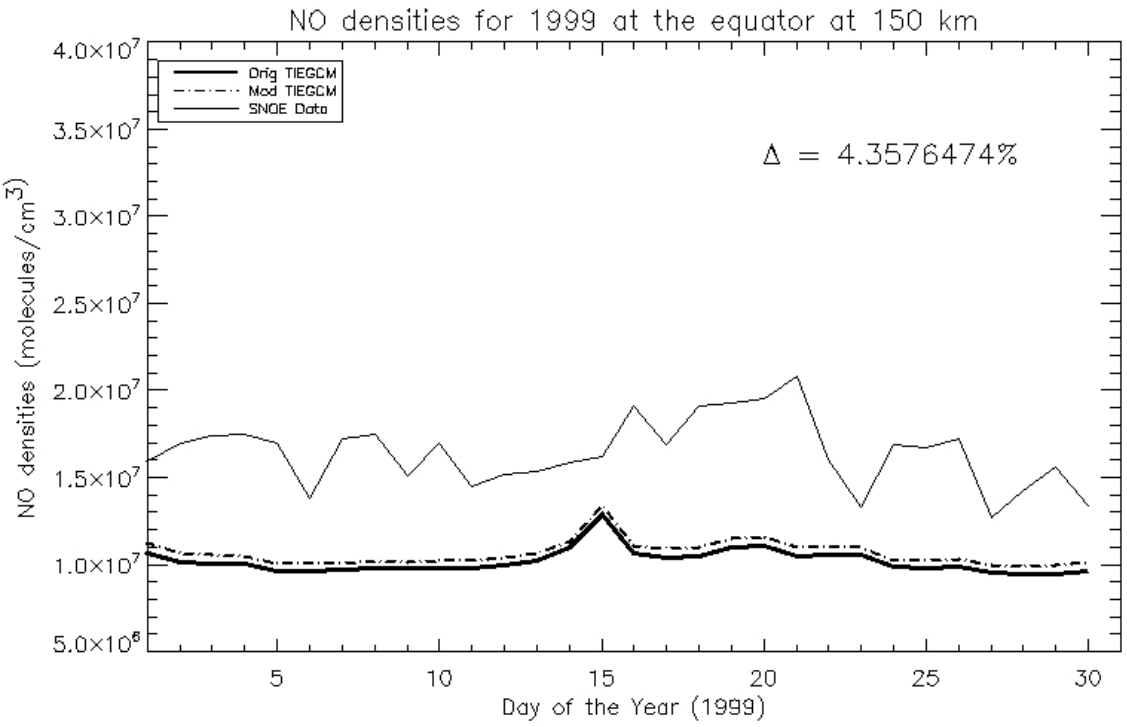

Figure 4.14: $N^+ + O_2 \rightarrow N(^2D) + O_2^+$, increased $N(^2D)$ yield

4.3.8 $N(^2D) + N_2 \rightarrow N(^4S) + N_2$

Similar to the loss of $N(^2D)$ to O to produce $N(^4S)$, this loss mechanism introduced to the model reduces NO densities at both altitudes. This efficiency of this loss mechanism also decreases with altitude, where quenching by O is the more prevalent form of loss for $N(^2D)$.

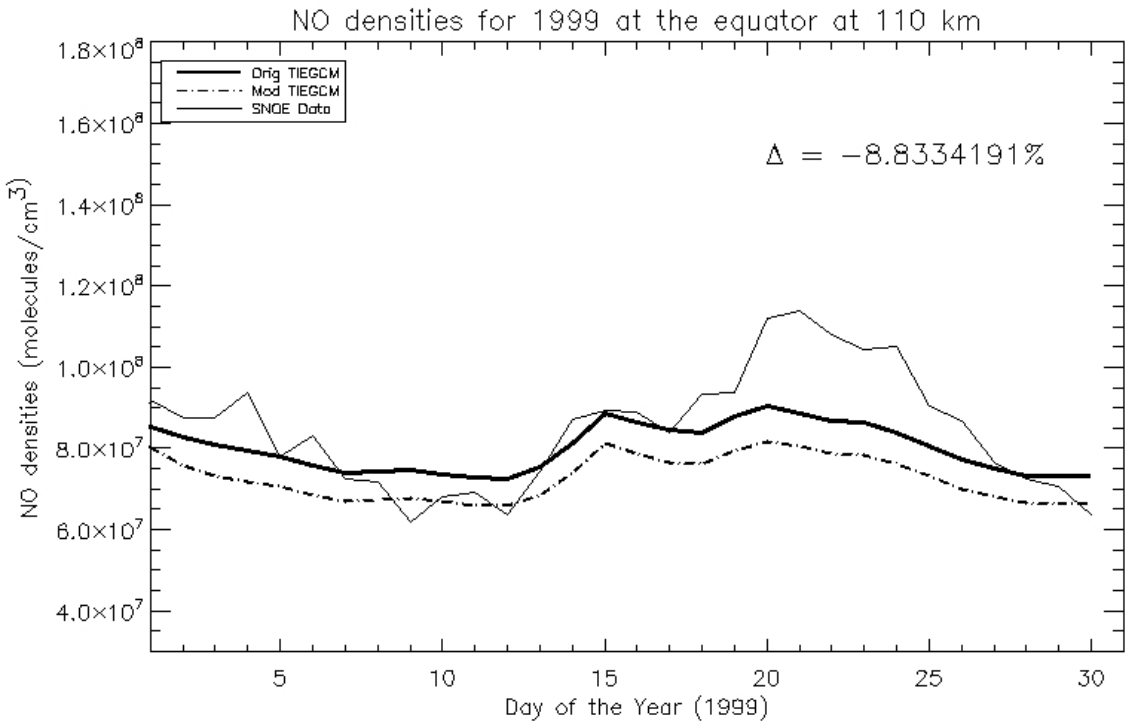

Figure 4.15: Introduced new reaction, effect at 110 km

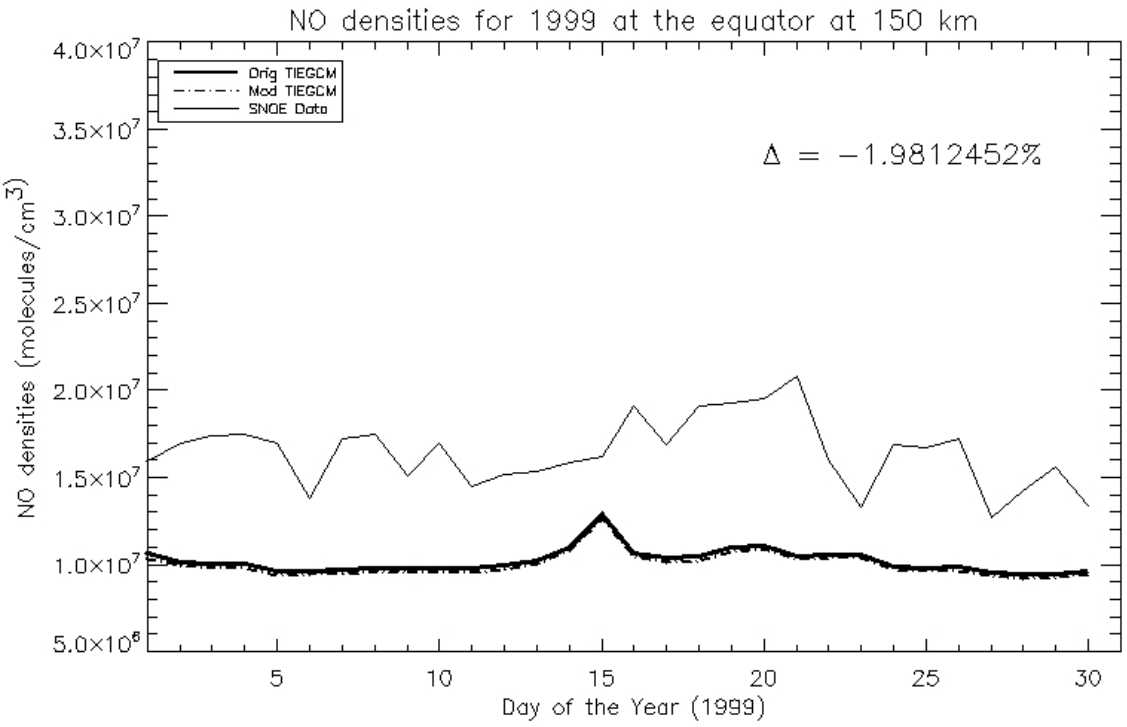

Figure 4.16: Introduced new reaction, effect at 150 km

4.3.9 $N_2(A)$ Chemistry, $N_2(A) + O \rightarrow NO + N(^2D)$

The aim of this thesis was to demonstrate the importance of $N_2(A)$ as a source of NO using the TIEGCM. It has been shown [8] that this reaction is important for accurately compensating for the NO peak when the branching ratio for $N(^2D)$ in the photodissociation of N_2 is reduced to 0.5. However, we see that this mechanism does not produce the expected increase in NO density at 110 km.

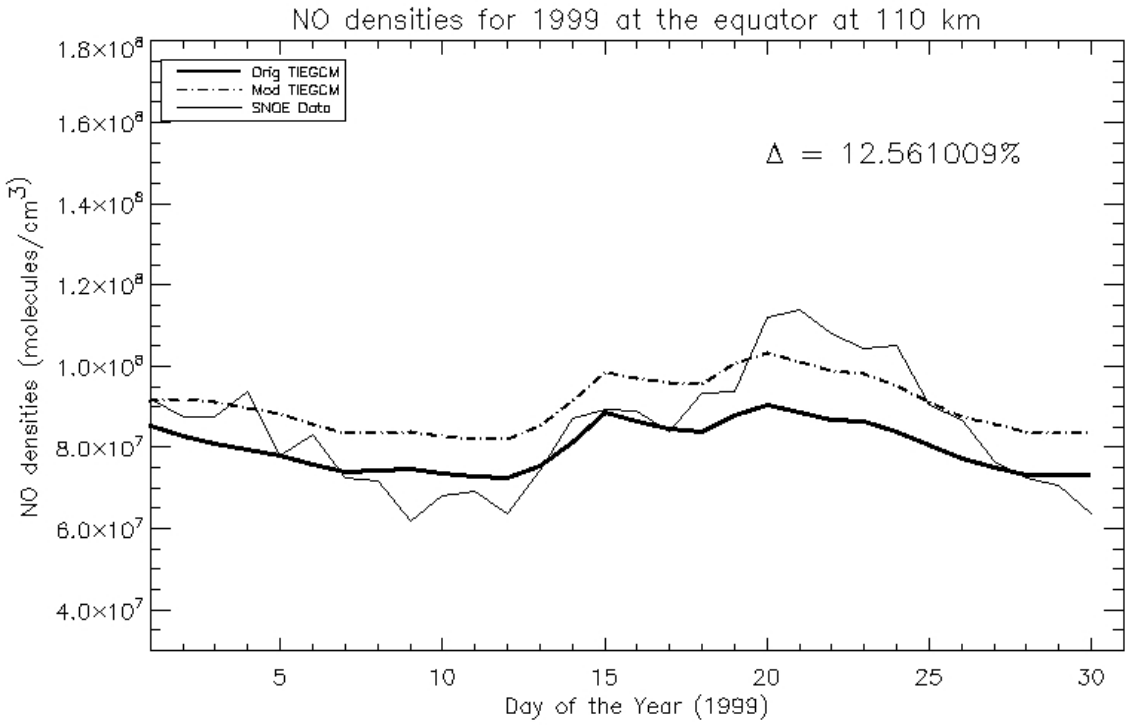

Figure 4.17: $N_2(A)$ chemistry, effect at 110 km

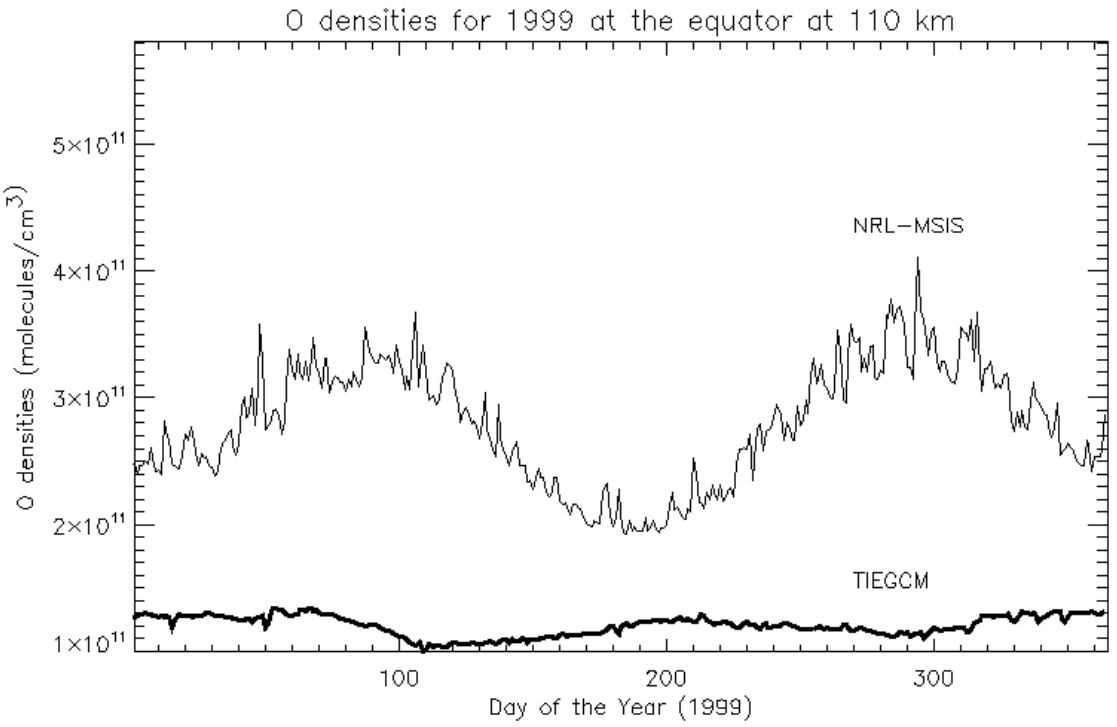

Figure 4.18: Atomic oxygen densities in NRL-MSIS & TIEGCM at 110 km

This is attributed to the difference in atomic oxygen densities as predicted by NRL-MSIS and the TIEGCM as shown in the plot above. We see that at 110 km atomic oxygen densities are more than 50% less than that predicted by NRL-MSIS. As this reaction of $N_2(A)$ is acutely dependent upon O densities, we do not see the required increase in NO densities at 110 km.

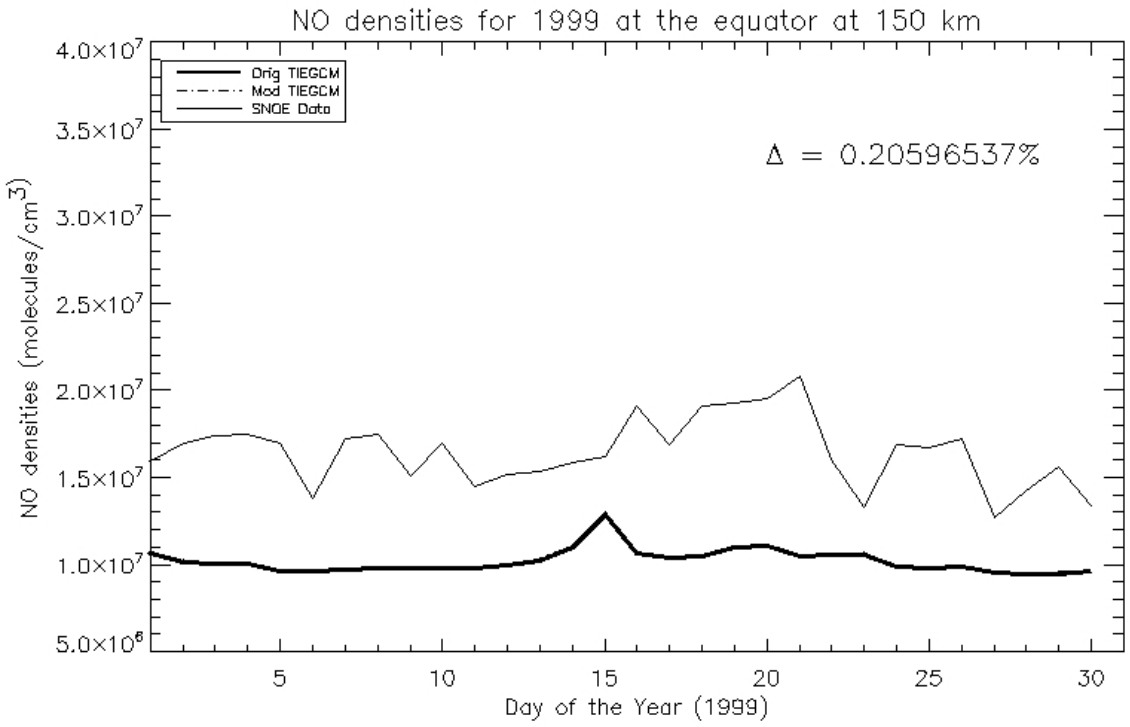

Figure 4.19: $N_2(A)$ chemistry, effect at 150 km

This reaction is a much greater contributor to NO densities at 110 km than at 150 km because of the short lifetime of N_2(A) (2 seconds) where it is decays to a lower energy state by radiation, instead of reacting with O.

4.3.10 Overall effect of updated chemistry

The plots below show the effect of the complete updated chemistry scheme being implemented in the TIEGCM. We see a decrease in the NO densities by 32% at 110 km while increasing it by 11% at 150 km. It should be noted that due to the non-linear nature of the chemistry, the sum of the effects of the individual changes is not equal to the effect of the whole chemistry scheme.

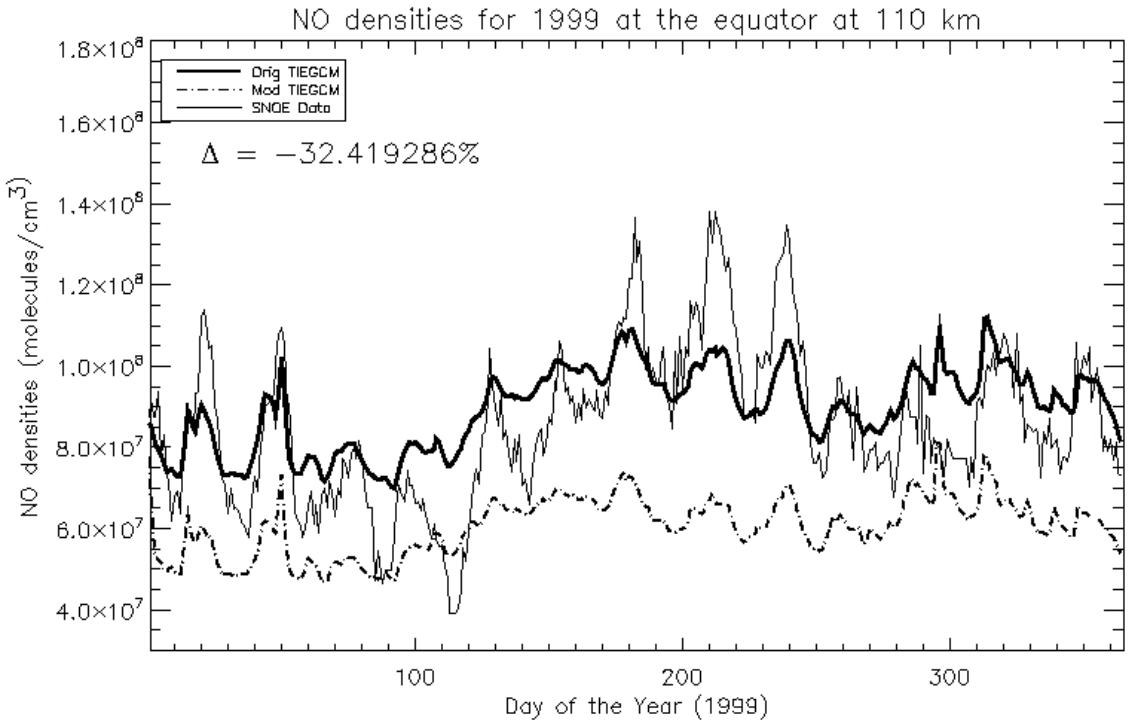

Figure 4.20: Updated chemistry scheme at 110 km

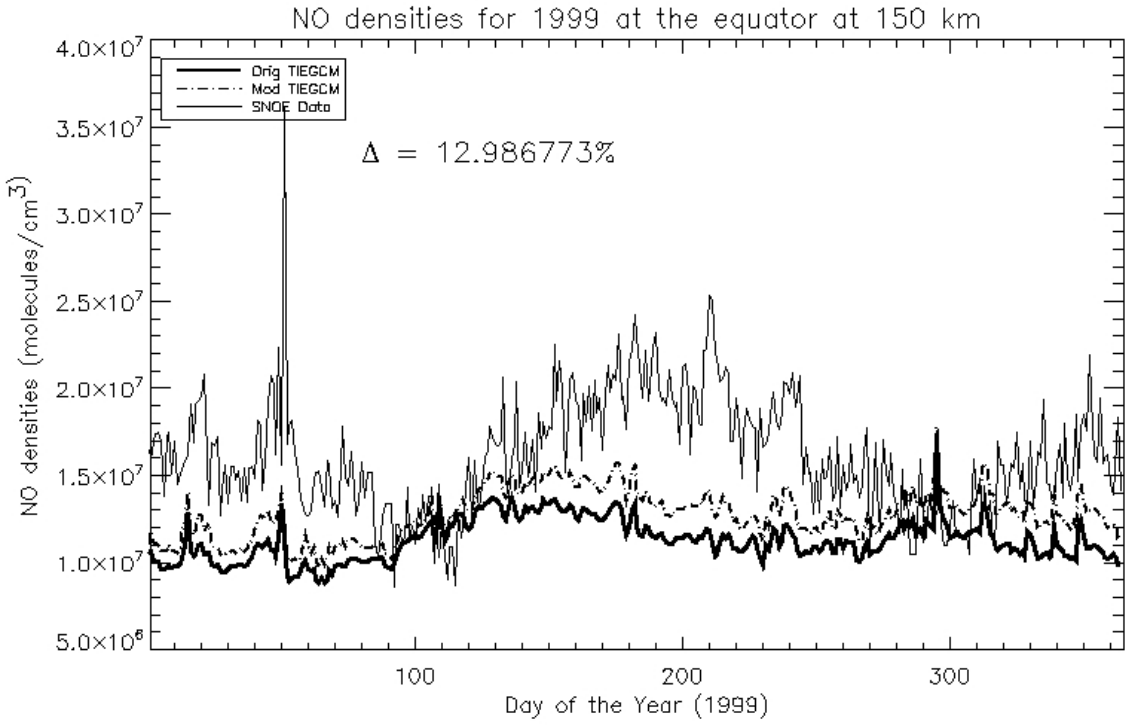

Figure 4.21: Updated chemistry scheme at 150 km

In trying to find the reason for the reduction in NO abundance at 110 km, we find that the neutral temperatures prediction is substantially different in the TIEGCM, as compared to the NRL-MSIS on which the chemistry scheme we use is based .

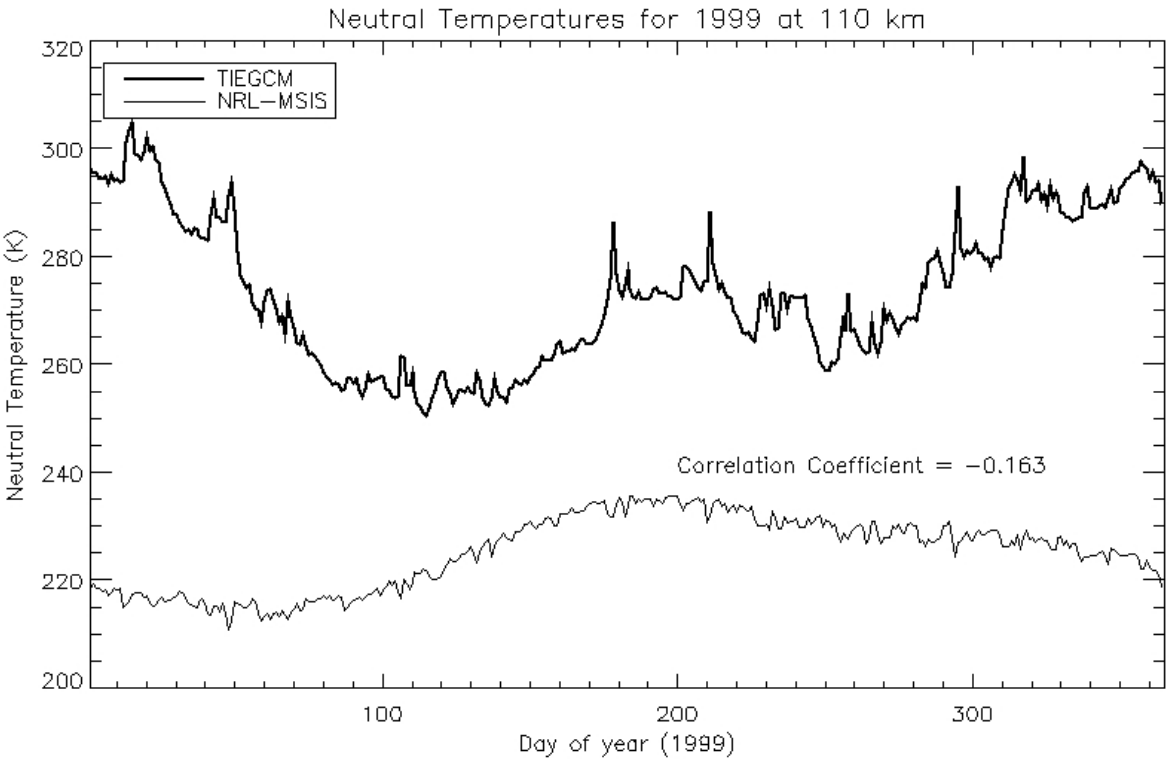

Figure 4.22: Comparison of neutral temperatures in NRL-MSIS and TIEGCM at 110 km

We see a negative correlation between the two temperatures at 110 km. The changes proposed through the presented chemistry scheme were based on parameters defined by the NRL-MSIS, as a result of which changes made to the TIEGCM negatively affects the NO densities even though the chemistry contained in the model has been improved. This can be seen at 150 km where the effects are more in line with our expectations where the neutral temeperature correlation between the two models is better.

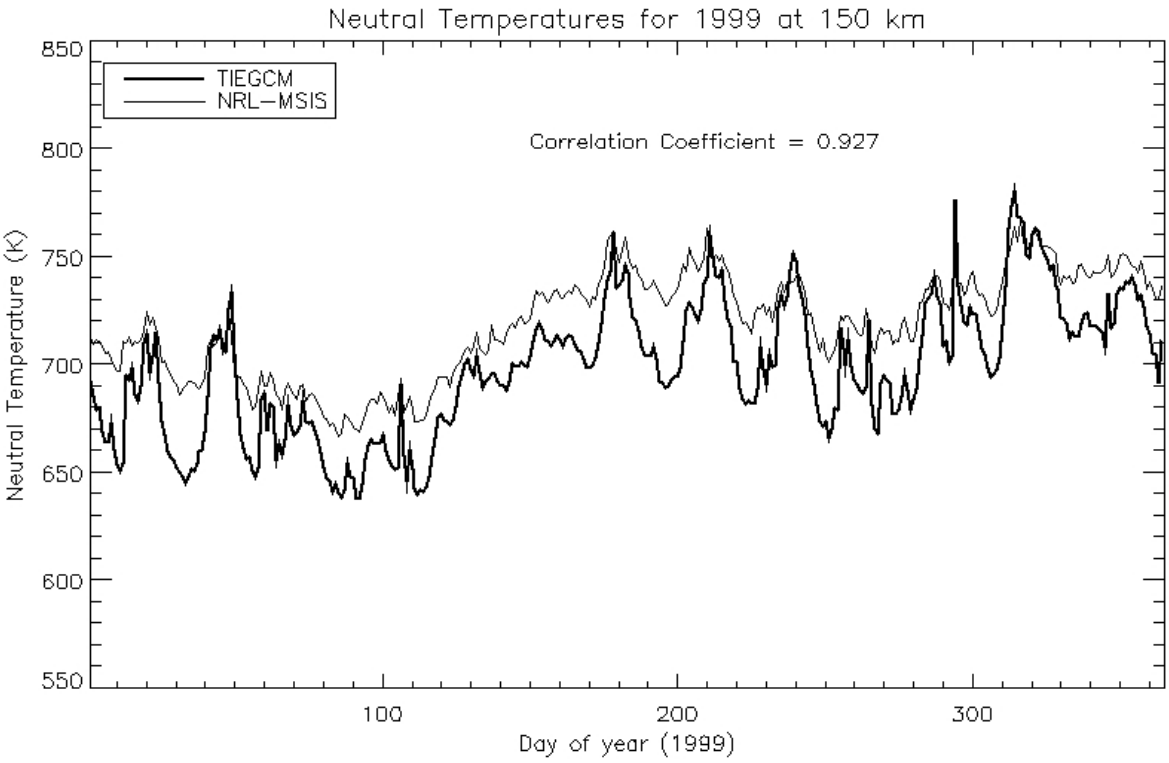

Figure 4.23: Comparison of neutral temperatures in NRL-MSIS and TIEGCM at 110 km

The updated chemistry scheme used here was implemented in the 1-D NO model and was shown to improve the agreement with SNOE data at both 110 km and 150 km [3]. However, as key aspects such as neutral temperatures and atomic oxygen densities in the TIEGCM are substantially different from those in the NRL-MSIS, we do not observe the same improvement as was seen in the 1-D model. Lab measurements of chemical rate coefficients provide a range of possible values rather than show consistent agreement on one particular value. The 1-D model results of Yonker et al. were achieved by choosing coefficients in the range allowed by lab data and producing optimal agreement with SNOE. Since TIEGCM is based on significantly different temperatures and O densities than those yielded by MSIS and used by the Yonker et al., it is necessary that we return to the lab constraints and repeat the procedure previously used, but with TIEGCM. Interestingly, changes to the NO densities will in turn affect the models neutral temperature calculations, as NO plays an important

role in thermospheric cooling. It will thus be necessary to iteratively obtain appropriate values for parameters affecting the chemistry that allow the model to better predict NO, while accounting for the effects of the changed NO densities due to the modified chemistry.

Chapter 5

Conclusions

We see that the changes made to the model have not improved the model's ability to predict NO densities in the expected manner. The overall abundance of NO is reduced by 32.5% at a 110 km while increasing the same at 150 km by about 13%. Though we have successfully implemented a chemistry scheme that we know from 1-D NO models to improve agreement with data, we were unable to achieve similar results with the TIEGCM.

We know from the use of 1-D NO models that a good agreement between the model and data can be achieved with the NO chemistry scheme that is used in this thesis [3]. The values that were used for various parameters in were obtained from experiments that defined the most likely limits for those parameters, while the exact values used were determined from the results obtained from the NO 1-D model that achieved a best fit with the SNOE data. These values hence, are not neccessarily those which would provide the best fit between the model and data in the TIEGCM. The difference between the NRL-MSIS and TIEGCM in predicting the neutral temperatures and atomic oxygen densities further contributes to this fact. Obtaining parameter values specific to the TIEGCM that improve this agreement would be the logical next step for this work.

The future work planned is to either reconcile the neutral temperatures of the two models,

or to implement the presented chemistry scheme in the light of the neutral temperature calculations of the TIEGCM. A more basic step would be to verify the neutral temperatures obtained from either model with actual data, which would indicate the appropriate course of action to be pursued.

Also proposed below are further changes required to the NO chemistry of the TIEGCM which were left unimplemented due to time and complexity constraints.

Table 5.1: Future TIEGCM Modifications

Code	Change	Reference	Expected Effect
`brn2DEl`	lower σ(PEDN2)	*Cosby(1993)*	Decrease NO since brn2d = 0.5
`rk9`	TD of $N_2^+ + O_2 \rightarrow N_2 + O_2^+$	*Fox(2003)*	Increase NO below 300K (110 km)
`deltaq`	$N(^2D) + O_2 \rightarrow NO(v) + 0.02\ O(^1D)$	*Miller(2004)*	Decrease in Neutral Temperature
`alfa_no`	Thermal Diffusion	*Yonker(CEDAR'08)*	Minor increase in NO diffusion
`alfa_n4s`	Thermal Diffusion	*Yonker(CEDAR'08)*	Minor decrease in $N(^4S)$ diffusion

As has been stressed upon in this thesis, obtaining and modelling NO accurately is essential to an accurate representation of the thermosphere. The TIEGCM being an open source model allows users to contribute to the process of making it better. Being a widely accepted thermospheric model in the atmospheric science community, the TIEGCM also serves partially as the basis for models such as the TIMEGCM, which extends the TIEGCM to include the mesosphere (a lower boundary of 32 km) and the WACCM (Whole Atmospher Community Climate model). Ensuring that the NO can be modelled sufficiently well using the TIEGCM will serve as a template upon which one can expand to other three dimensional atmospheric models.

Bibliography

[1] A. D. Richmond, E. C. Ridley, and R. G. Roble, "A thermosphere/ionosphere general circulation model with coupled electrodynamics," *GRL*, vol. 19, pp. 601–604, Mar. 1992.

[2] S. C. Solomon, C. A. Barth, P. Axelrad, S. M. Bailey, R. Brown, R. L. Davis, T. E. Holden, R. A. Kohnert, F. W. Lacy, M. T. McGrath, D. C. O'Connor, J. P. Perich, H. L. Reed, M. A. Salada, J. Simpson, J. M. Srinivasan, G. A. Stafford, S. R. Steg, G. A. Tate, J. C. Westfall, N. R. White, P. R. Withnell, and T. N. Woods, "Student Nitric Oxide Explorer," in *Society of Photo-Optical Instrumentation Engineers (SPIE) Conference Series* (E. K. Casani & M. A. Vander Does, ed.), vol. 2810 of *Society of Photo-Optical Instrumentation Engineers (SPIE) Conference Series*, pp. 121–132, Oct. 1996.

[3] S. M. Bailey, C. A. Barth, and S. C. Solomon, "A model of nitric oxide in the lower thermosphere," *Journal of Geophysical Research (Space Physics)*, vol. 107, p. 1205, Aug. 2002.

[4] C. A. Barth, W. K. Tobiska, D. E. Siskind, and D. D. Cleary, "Solar-terrestrial coupling - Low-latitude thermospheric nitric oxide," *GRL*, vol. 15, pp. 92–94, Jan. 1988.

[5] C. A. Barth, "Nitric oxide in the lower thermosphere," *Planetary and Space Science*, vol. 40, pp. 315–336, Feb. 1992.

[6] R. E. Dickinson, E. C. Ridley, and R. G. Roble, "A three-dimensional general circulation model of the thermosphere," *JGR*, vol. 86, pp. 1499–1512, Mar. 1981.

[7] R. G. Roble, E. C. Ridley, A. D. Richmond, and R. E. Dickinson, "A coupled thermosphere/ionosphere general circulation model," *GRL*, vol. 15, pp. 1325–1328, Nov. 1988.

[8] J. D. Yonker and S. M. Bailey, "Dayglow Production of NO at 110 km," 2012. Document under preparation.

[9] F. Hellberg, S. Rosén, R. Thomas, A. Neau, M. Larsson, A. Petrignani, and W. J. van der Zande, "Dissociative recombination of NO^+: Dynamics of the X $^1\Sigma^+$ and a $^3\Sigma^+$ electronic states," *JCP*, vol. 118, pp. 6250–6259, Apr. 2003.

[10] J. R. Peterson, A. L. Padellec, H. Danared, G. H. Dunn, M. Larsson, A. Larson, R. Peverall, C. Strömholm, S. Rosén, M. af Ugglas, and W. J. van der Zande, "Dissociative recombination and excitation of N_2^+: Cross sections and product branching ratios," *The Journal of Chemical Physics*, vol. 108, no. 5, pp. 1978–1988, 1998.

[11] E. C. Zipf and R. W. McLaughlin, "On the dissociation of nitrogen by electron impact and by EUV photo-absorption," *Planetary and Space Science*, vol. 26, pp. 449–462, May 1978.

[12] D. E. Siskind, D. J. Strickland, R. R. Meier, T. Majeed, and F. G. Eparvier, "On the relationship between the solar soft X ray flux and thermospheric nitric oxide: An update with an improved photoelectron model," *JGR*, vol. 1001, pp. 19687–19694, Oct. 1995.

[13] S. P. Sander, R. R. Friedl, D. M. Golden, M. J. Kurylo, G. K. Moortgat, H. Keller-Rudek, P. H. Wine, A. R. Ravishankara, C. E. Kolb, M. J. Molina, B. J. Finlayson-Pitts, R. E. Huie, and Orkin, "Chemical Kinetics and Photochemical Data for Use in Atmospheric Studies, Evaluation Number 15," *JPL Publication 06-02*, 2006.

[14] J. Herron, "Evaluated Chemical Kinetics Data for Reactions of $N(^2D)$ $N(^2P)$, and $N_2(A^3\Sigma^+{}_u)$ in the Gas Phase," *Journal of Physical and Chemical Reference Data*, vol. 28, p. 1453, Sept. 1999.

[15] J. W. Duff, H. Dothe, and R. D. Sharma, "On the rate coefficient of the N(^{2}D)+O_2->NO+O reaction in the terrestrial thermosphere," *GRL*, vol. 30, pp. 050000–1, Mar. 2003.

[16] A. J. Midey, A. A. Viggiano, P. Zhang, S. Irle, and K. Morokuma, "A Study of the Reaction of N^+ with O_2: Experimental Quantification of NO^+(a 3+) Production (298500 K) and Computational Study of the Overall Reaction Pathways," *The Journal of Physical Chemistry A*, vol. 110, no. 9, pp. 3080–3086, 2006. PMID: 16509629.

[17] J. M. Thomas and F. Kaufman, "An Upper Limit on the Formation of NO(X2r) in the Reactions + O(3P) and + at 298 K," *The Journal of Physical Chemistry*, vol. 100, no. 21, pp. 8901–8906, 1996.

[18] L. Campbell, D. C. Cartwright, and M. J. Brunger, "Role of excited N_2 in the production of nitric oxide," *Journal of Geophysical Research (Space Physics)*, vol. 112, p. 8303, Aug. 2007.